Electronic Origin of the Stability of Transition Metal Doped B_{14} Drum Shaped Boron Clusters and their Assembly in to a Nanotube

Pinaki Saha[1], Amol B. Rahane[2], Vijay Kumar[2,3], N. Sukumar[1,3]*

[1]Department of Chemistry, School of Natural Sciences, Shiv Nadar University, NH-91, Tehsil Dadri, Gautam Buddha Nagar 201314, U.P., India

[2]Dr. Vijay Kumar Foundation, 1969, Sector 4, Gurgaon 122001, Haryana, India

[3]Center for Informatics, School of Natural Sciences, Shiv Nadar University, NH-91, Tehsil Dadri, Gautam Buddha Nagar 201314, U.P., India

*Corresponding author

ABSTRACT: We study the stability of drum-shaped transition metal (TM) doped boron clusters, $M@B_n$ with n = 14 and 16, and M = 3*d*, 4*d*, and 5*d* TM atom using *ab initio* calculations. Our results show that drum-shaped $M@B_{14}$ clusters are favored for M = Cr, Mn, Fe, Co, and Ni, while in other cases, open conical or bowl shaped structures become more favorable. The isoelectronic $Ni@B_{14}$ and $Co@B_{14}^-$ clusters have large highest occupied molecular orbital-lowest unoccupied molecular orbital (HOMO-LUMO) gaps and these are magic clusters. Their stability has been

correlated with the occurrence of magic behavior with 24 valence electrons in a disk jellium model while for $Fe@B_{14}$ case, the drum structure is deformed and the stability occurs at 22 delocalized valence electrons. The bonding nature in these clusters has been studied by analyzing the electron density at bond and ring critical points, the Laplacian distribution of the electron density, the electron localization function, the source function, and electron localization-delocalization indices, all of which suggest two and three-center σ bonding within and between the two B_7 rings, respectively, and hybridization between the TM *d* orbitals and the π bonded molecular orbitals of the drum. The infrared and Raman spectra of these magic clusters show all real frequencies, suggesting the dynamical stability of the drum-shaped structures. There is a low frequency mode associated with the M atom. Results of the electronic spectra of the anion clusters are also presented that may help to identify these species in future experiments. Further, we discuss the stability of 24 delocalized valence electron systems $Mn@B_{16}$ anion, $Fe@B_{16}$, $Co@B_{16}$ cation, and other related clusters. Assembly of $Co@B_{14}$ clusters has been shown to stabilize a carbon nanotube-like nanotube of boron with Co atomic nanowire inside while a nanotube of boron with triangular network has been obtained with the assembly of $Fe@B_{16}$ drum-shaped clusters. Both the nanotubes are metallic.

1. Introduction

Recent developments of novel atomic structures of boron clusters have generated great interest in the understanding of their growth behavior and the underlying bonding characteristics. In the relatively small size range B_n ($n < 40$), clusters generally have planar and quasi-planar structures[1-2], while a fullerene-like cage structure has been found to be of the lowest energy for neutral B_{40}

but a quasi-planar structure of B_{40} anion[3] is favored over the fullerene structure. Therefore, cage and planar/quasi-planar structures compete in this size range. Cage structures have also been reported[4,5] for B_{39} and B_{28} while for larger sizes, core shell structures have been reported[6] for B_{68}, B_{74}, and B_{80}. On the other hand, B_{84} again favors a quasi-planar structure with hexagonal holes in an otherwise triangular network.[7] Double ring tubular structures have also been reported[8,9] in some cases such as B_{20} and B_{24}. Therefore, boron clusters take up different shapes for different sizes, unlike the case of carbon where fullerene and nanotube structures are prevalent. Doping of a metal (M) atom could further lead to novel structures, as has been shown for M doped silicon clusters.[10,11] Indeed recent experiments on M doped boron clusters[12,13] showed the formation of $Mn@B_{16}$ and $Co@B_{16}$ anions, which have been suggested to have drum shaped structures with the M atom inside, though elemental B_{16} cluster has a planar structure.[14] These results give credence to the idea that the interaction of a transition M (TM) atom with an aggregate of another element A such as those of Al, Au, Si, Ge, Sn, … leads to novel cage structures of A, pure clusters of which may not have cage structures.[15] Here the stability of a small boron cage mediated by the π bonded molecular orbitals can be increased by the doping of TM atom[16-17] and give rise to new possibilities. Recently a B_{24} cage has also been obtained with the doping of a Mo atom[17], while Saha *et al*.[18] have studied small doped boron clusters and have found magic behavior for disk-shaped clusters with effectively 12 delocalized valence electrons. It was shown that B_{11} has large electron affinity (EA) while B_{11} anion has a large highest occupied molecular orbital-lowest unoccupied molecular orbital (HOMO-LUMO) gap. Recent experiments[19] show large EA of 3.401 eV for B_{11} and low EA of 2.221 eV for B_{12}.

In this paper, we explore the effects of doping of a 3*d*, 4*d*, and 5*d* TM atom on the atomic structure and stability of B_{14} and B_{16} clusters. In particular, we look for the M atoms and the size of a boron

cluster for which the M doped boron drum structure is favorable. We have performed further analysis of the stability in the cases for which the TM atom favors the drum structure to be of the lowest energy. It is found that the doping of a 3*d* TM atom in B_{14} double ring tubular structure (Figs. 1 and 2) gives rise to large HOMO-LUMO gaps, in particular for neutral $Cr@B_{14}$, $Fe@B_{14}$, and $Ni@B_{14}$ for which the values are 1.31 eV, 1.30 eV, and 1.73 eV, respectively. The tubular isomer is lower in energy compared to an isomer in which the TM atom interacts with a bowl shaped B_{14} cluster, a planar isomer with the M atom embedded in the boron network, and a conical isomer. Note that B_{14} and B_{16} clusters have a planar structure among the low lying isomers, and for B_{14} a cage-like structure has slightly lower energy.[14,20] Therefore, upon doping of M atom, the structures of the doped clusters become quite different from those of the elemental boron clusters. We have also studied anions and cations of Mn and Co doped boron clusters, respectively, for which a tubular structure is favored. However, for the doping of 4*d* and 5*d* elements, as well as other 3*d* TM atoms, a bowl-shaped isomer is lower in energy as compared to a tubular (drum) structure. Further, in most cases of $M@B_{16}$ clusters, the HOMO-LUMO gap is generally small and in a few cases the drum structure has relatively large HOMO-LUMO gap such as for M = Fe and some charged clusters. Our results suggest that Cr, Mn, Fe, Co, and Ni atoms have the right size to stabilize B_{14} tubular structure, though Fe, Co, and Ni are optimal in the sense that the binding energy of the doped clusters is increased compared to the value for the elemental B_{14} cluster. We correlate the stability of Ni doped B_{14} cluster with the occurrence of magic behavior in a disk jellium model[21,22] at 24 valence electrons and discuss the trends obtained in the variation of the properties of the double ring tubular structures doped with different 3*d* TM atoms. Further we have studied TM doped B_{16} clusters and besides the stability of the structures for different TM atoms, we present results on $Mn@B_{16}$ anion, $Fe@B_{16}$, $Co@B_{16}$ cation, and other similar 24 delocalized

valence electron drum shaped clusters. Finally, we show that these drum-shaped clusters can be assembled in to a nanotube. This is similar to the nanotube structure of silicon[10,11] and germanium[23,24] that were shown to be stabilized by doping of M atoms. However, we find a carbon-like nanotube of boron by assembling $Co@B_{14}$ drum-shaped clusters and it is stabilized by an atomic wire of Co inside. Also, another tubular structure has been obtained by assembling $Fe@B_{16}$ drum-shaped clusters that has a triangular network of boron atoms.

2. Method of Calculation

The calculations have been performed using density functional theory with generalized gradient approximation (GGA) of Perdew, Burke, and Ernzerhof (PBE)[25] for the exchange-correlation energy. The electron-ion interaction is treated with the projector augmented wave (PAW) pseudopotential method[26] using the Vienna *Ab initio* Simulation Package (VASP).[27] We used medium precision to expand the wave function in a plane wave basis. The calculations were considered to be converged when the absolute value of the force on each ion was less than 0.005 eV $Å^{-1}$ with a convergence for the total energy of about 10^{-5} eV without any symmetry constraint. A cubic supercell with lattice parameter of 20 Å was used and the gamma point for Brillouin zone integrations for all calculations on clusters. Further calculations with PBE0 functional have been performed using the Gaussian09 program[28] and 6-311+G basis set for the most favourable cases of the drum structure. The same has also been used to calculate the infrared (IR) spectra and Raman activity for Fe, Co, and Ni doped drum structures. In all these cases, we find real frequencies suggesting the dynamical stability of the structures. For the infinite nanotube structures, we optimized the interatomic spacing by fully relaxing the ions. We used 17 k-points along the nanotube axis for Brillouin zone integrations and 100 k-points to plot the energy bands. Spin-

polarized calculations have been performed in many cases in order to check if the lowest energy isomer has any magnetic moments.

Further analysis of the electron density has been performed by calculating the Laplacian distribution $L(\mathbf{r})=-\frac{1}{4}\nabla^2\rho(\mathbf{r})$ and source function[29-32] at bond critical points (BCPs) and ring critical points (RCPs), using the AIMAll[33] program, electron localization-delocalization indices with the AIMLDM[34] script, as well as electron localization function (ELF) from VASP calculations to infer the bonding characteristics in these clusters. The source function $S(\mathbf{r},\Omega)$ was employed to measure the relative contribution of an atom or a group of atoms to the density at any point **r**. The local source function is given as:

$$LS(\mathbf{r}, \mathbf{r'}) = \frac{-1}{4\pi}\frac{\nabla^2\rho(\mathbf{r'})}{|\mathbf{r}-\mathbf{r'}|} \quad (1),$$

and it represents the effectiveness of the Laplacian function $L(\mathbf{r'})$ at **r'** in functioning as a source (or sink) for the electron density at **r** modulated by the Green's function $(4\pi|\mathbf{r}-\mathbf{r'}|)^{-1}$. Thus, the Laplacian also serves as the generator of the electron density distribution, by virtue of Poisson's equation:

$$\rho(\mathbf{r}) = \frac{-1}{4\pi}\int d\mathbf{r'}\frac{\nabla^2\rho(\mathbf{r'})}{|\mathbf{r}-\mathbf{r'}|} \quad (2).$$

Equation (1) may be rewritten as:

$$LS(\mathbf{r}, \mathbf{r'}) = \frac{-1}{\pi}\frac{2G(\mathbf{r'}) + V(\mathbf{r'})}{|\mathbf{r}-\mathbf{r'}|} \quad (3),$$

where $G(\mathbf{r})$ and $V(\mathbf{r})$ are the kinetic energy density and potential energy, respectively. Any region where the electron density is locally concentrated ($\nabla^2\rho(\mathbf{r'}) < 0$) and where the potential energy dominates the kinetic energy, acts as a source for the electron density at other points, while a region

where the electron density is locally depleted ($\nabla^2\rho(\mathbf{r'}) > 0$) and where the kinetic energy dominates acts as a sink, removing electron density from **r**.

The integral of the local source function over the basin Ω of an atom or functional group is the source function $S(\mathbf{r}, \Omega)$ that represents contribution from that atom or functional group to $\rho(\mathbf{r})$:

$$S(\mathbf{r}, \Omega) = \int_\Omega LS(\mathbf{r}, \mathbf{r'})\, d\mathbf{r'} \qquad (4).$$

Thus $$\rho(\mathbf{r}) = \int_\Omega LS(\mathbf{r}, \mathbf{r'})\, d\mathbf{r'} + \sum_{\Omega' \neq \Omega} \int_{\Omega'} LS(\mathbf{r}, \mathbf{r'})\, d\mathbf{r'}$$

$$= S(\mathbf{r}, \Omega) + \sum_{\Omega' \neq \Omega} S(\mathbf{r}, \Omega') \qquad (5).$$

The electron density at any point in an atom is thus decomposed into a contribution arising from sources within the basin of the atom and a contribution arising from sources external to the atom. The source function is a measure of the relative contribution of an atom or group of atoms to the electron density at any point.

The density of the Fermi hole is the difference between the pair density for electrons $P^{\alpha\alpha}(\mathbf{r}_1,\mathbf{r}_2)$ of the same spin (denoted here by α), and the simple product of the one-particle densities; it describes how the density of a reference electron at any point in space spreads out into the space of another electron of the same spin, thereby excluding an identical amount of same spin density:

$$\rho_x^{\alpha}(\mathbf{r}_1,\mathbf{r}_2) = P^{\alpha\alpha}(\mathbf{r}_1,\mathbf{r}_2) - \rho^{\alpha}(\mathbf{r}_1)\rho^{\alpha}(\mathbf{r}_2) \qquad (6).$$

Double integration of this quantity over the coordinates of both electrons in the basin of an atom Ω_A gives the Fermi correlation within that atom A:

$$F^{\alpha}(A,A) = \int_{\Omega A} \int_{\Omega A} \rho_x^{\alpha}(\mathbf{r}_1,\mathbf{r}_2)\, d\mathbf{r}_1 d\mathbf{r}_2 \qquad (7).$$

The localization index $\lambda(A)$ is thus defined as:

$$\lambda(A) = |F^{\alpha}(A,A) + F^{\beta}(A,A)| = \int_{\Omega A}\int_{\Omega A} \rho_x(\mathbf{r}_1,\mathbf{r}_2)\, d\mathbf{r}_1 d\mathbf{r}_2 \quad (8).$$

Conversely the exchange of electrons between the basins of atoms A and B is given by:

$$F^{\alpha}(A,B) = \int_{\Omega A}\int_{\Omega B} \rho_x{}^{\alpha}(\mathbf{r}_1,\mathbf{r}_2)\, d\mathbf{r}_1 d\mathbf{r}_2 \quad (9),$$

which is then used to define the delocalization index $\delta(A,B)$:

$$\delta(A,B) = |F^{\alpha}(A,B) + F^{\beta}(A,B)| = \int_{\Omega A}\int_{\Omega B} \rho_x(\mathbf{r}_1,\mathbf{r}_2)\, d\mathbf{r}_1 d\mathbf{r}_2 \quad (10).$$

The localization and delocalization indices account for the whereabouts of the total electron population (N); the former counts the number of electrons localized within an atomic basin, while the latter counts the number of electrons shared between two atomic basins. Both these quantities are combined in the localization-delocalization matrix (LDM)[35], which contains λ along the diagonals, and half of δ in the off-diagonal elements. The sum of any column or row then yields the resulting atomic population:

$$N(A) = \lambda(A) + \tfrac{1}{2}\sum_{B\neq A} \delta(A,B) \quad (11).$$

LDM thus captures information on both localization of electrons into atomic basins (in its diagonal elements) and electrons shared between pairs of atoms (whether "bonded" or not).

A local measure of electron localization, also derived from the Fermi hole, is ELF, introduced by Becke and Edgecombe[36]:

$$ELF(\mathbf{r}) = \{1 + [\Delta(\mathbf{r})/\Delta_0(\mathbf{r})]^2\}^{-1} \quad (12),$$

Where $\Delta(\mathbf{r})$ is a measure of the local excess kinetic energy due to Pauli repulsion:

$$\Delta(\mathbf{r}) = G(\mathbf{r}) - T_w(\mathbf{r}) \quad (13),$$

$T_w(\mathbf{r})$ is the Weiszäcker kinetic energy density, and $\Delta_0(\mathbf{r})$ is the kinetic energy of a uniform electron gas with density $\rho(\mathbf{r})$. ELF($\mathbf{r}$) varies in the range [0,1] and increases with increasing electron localization, with ELF = 1 corresponding to perfect localization.

3. Results and Discussion

3.1 Magic Clusters and Their Atomic Structures. We started the search for optimum small size drum-shaped boron structures that may be able to accommodate a TM atom, by considering boron clusters with 10, 12, 14, and 16 atoms having two equal polygonal boron rings placed in staggered configuration, such that boron atoms form a triangular network that is generally favorable. We placed different TM atoms in between the rings. Optimization of these structures showed that the initial drum-shaped structures with 10 and 12 atoms deformed very much due to the inability of these small boron clusters to accommodate M atom in the tubular cavity. The optimized structures are shown in Supplemental Information in Tables S1 and S2. The HOMO-LUMO gaps of these structures are also small suggesting low chemical stability and that larger clusters may be more appropriate and favorable.

We moved onto larger sizes with 14 and 16 boron atoms. ln the case of M doped B_{14} and B_{16} clusters, we find that the drum-shaped structure is retained in most cases of 3*d* TM atoms and in the case of Cr, Mn, Fe, Co, and Ni, it is the most stable structure (see Fig. 1), but the doping of 4*d* and 5*d* TM atoms in these clusters leads to significant distortion in some cases (see Tables S3, S4, and S5 in Supplemental Information). In the optimizations of B_{14} drum-shaped structures doped with a 3d TM atom, we studied different spin-isomers, but for Cr, Mn, Fe, Co, and Ni doping a singlet (doublet) state was favored for TM atom having even (odd) number of electrons. In general,

the HOMO-LUMO gap of the M doped B_{16} clusters is small (see Table S5), while the M doped B_{14} clusters have *large* HOMO-LUMO gap (1-1.8 eV within GGA) and *zero magnetic moment* in some cases. In a few cases of M doped B_{16} clusters also, we find relatively large HOMO-LUMO gaps (~0.8 eV within GGA) and non-zero magnetic moments indicative of M doped boron *radicals*. We shall discuss these cases later. A large HOMO-LUMO is indicative of the chemical stability of such doped clusters. Note that the true HOMO-LUMO gap would be higher, as it is underestimated in GGA. We also obtained large HOMO-LUMO gaps (see discussion later) when calculations were performed using PBE0 functional. These results led us to conclude that B_{14} drum structure is optimal for the doping of some of the 3*d* TM atoms in small boron clusters. Accordingly, we present results of 3*d* TM atom doped B_{14} clusters in detail. Further results of TM atom doped B_{16} clusters are given with a focus on the stability of clusters with effectively 24 valence electrons.

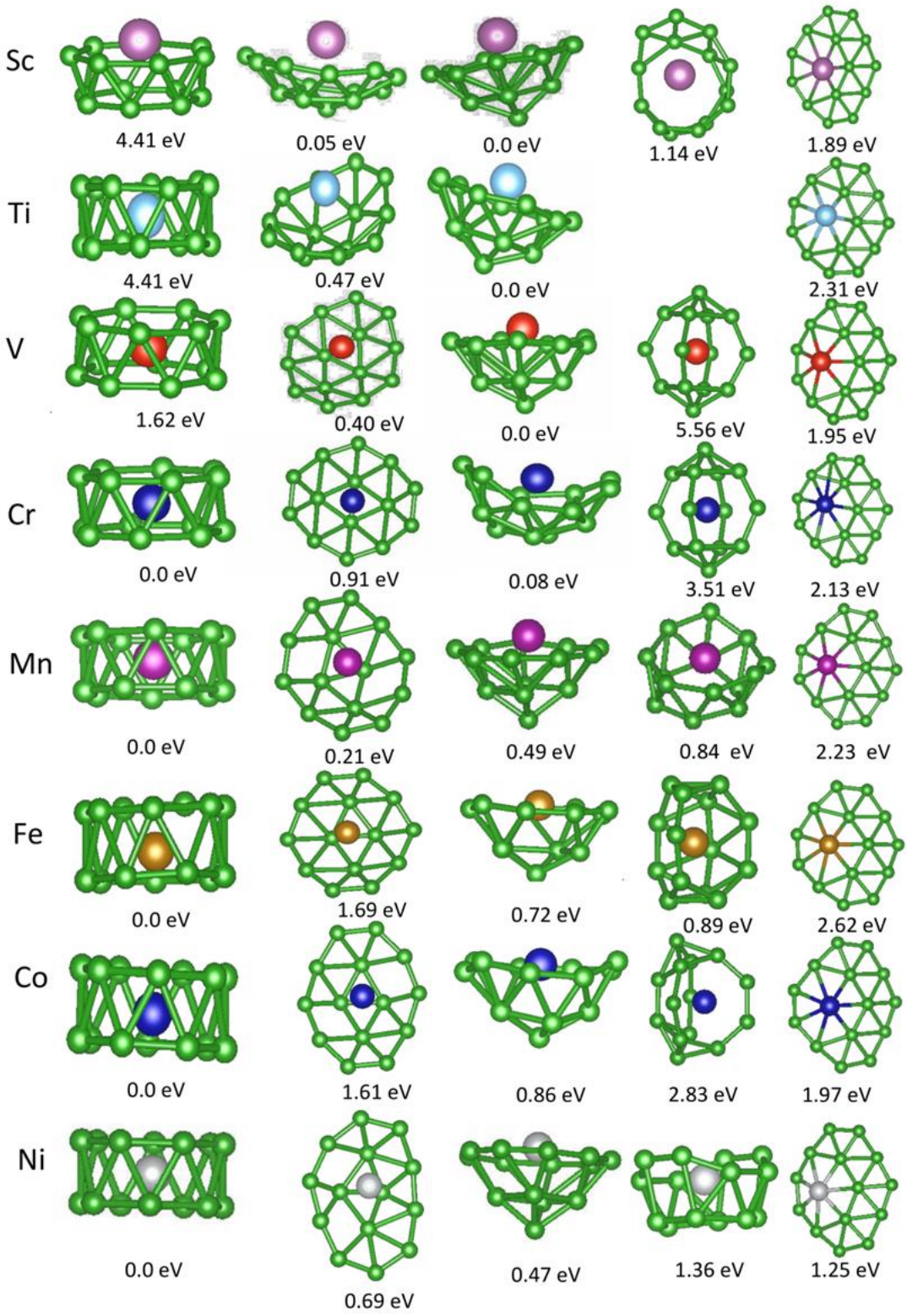
Sc
4.41 eV
0.05 eV
0.0 eV
1.14 eV
1.89 eV
Ti
4.41 eV
0.47 eV
0.0 eV
2.31 eV
V
1.62 eV
0.40 eV
0.0 eV
5.56 eV
1.95 eV
Cr
0.0 eV
0.91 eV
0.08 eV
3.51 eV
2.13 eV
Mn
0.0 eV
0.21 eV
0.49 eV
0.84 eV
2.23 eV
Fe
0.0 eV
1.69 eV
0.72 eV
0.89 eV
2.62 eV
Co
0.0 eV
1.61 eV
0.86 eV
2.83 eV
1.97 eV
Ni
0.0 eV
0.69 eV
0.47 eV
1.36 eV
1.25 eV

Figure 1. Atomic structures of some low-lying isomers of B_{14} clusters doped with a 3*d* TM atom. The drum-shaped structure is the lowest in energy for M = Cr, Mn, Fe, Co, and Ni. For large size M atoms (Sc, Ti, and V), open quasi-planar (bowl-shaped) or conical structures become more favorable than the drum structure. In the conical structure the M atom is in some cases surrounded by a ring of B atoms. Isomers obtained from fullerene-like structure or M atom in a boron network lie high in energy. For Ti, the fullerene-like structure transforms into a conical structure.

In our effort to find the lowest energy structures, we tried five initial structures as shown in Fig. 1 for 3*d* TM atoms doped in B_{14}. These structures are quasi-planar, drum-shaped, conical, fullerene-like and M atom embedded in a quasi-planar boron network. As small boron clusters tend to have triangular planar structures and for B_{14} a fullerene-like cage is slightly lower in energy, we tried to place a TM atom on the planar structure, which led to bowl shaped and conical structures. On the other hand, the fullerene-like isomer led to distorted structures. A drum-shaped isomer as well as an isomer with the M atom in a heptagonal hole in a planar boron network was also considered. As mentioned earlier, in the case of $M@B_{14}$ clusters (M = 4*d* and 5*d* TM atom), the drum-shaped structure is not of the lowest energy as 4*d* and 5*d* TM atoms are bigger in size compared with the 3*d* TM atoms. Our results show that in these cases conical or bowl-shaped structures are more favorable (Tables S3 and S4), as we also find for the larger 3*d* TM atoms such as Sc, Ti, and V (Fig. 1). In these cases, such as for M = Ti, the HOMO-LUMO gap is small and therefore these bowl and conical structures are chemically less stable; and it is likely that these structures may prefer more B atoms. Also in the case of the drum structures of $Sc@B_{14}$ and $Ti@B_{14}$, higher spin isomers with 3 μ_B and 2 μ_B magnetic moments are lower in energy, respectively. For 4*d* and 5*d* TM atoms, the structures are shown in Tables S3 and S4 in Supplemental Information. As

mentioned earlier, the M doped drum-shaped structure is the lowest energy isomer for M = Cr, Mn, Fe, Co, and Ni. A planar isomer in which the M atom is embedded in the boron network becomes quasi-planar and it is not of the lowest energy. These results suggest that the relatively small 3*d* TM atoms have the correct size to favor the cavity of tubular B_{14} that has the lowest energy. We calculated the binding energy, doping energy, and embedding energy for the boron clusters doped with 3*d* TM atoms. The binding energy for a cluster is defined as the energy per atom of the cluster with reference to free atoms, while the doping energy is defined as the lowering of the energy due to the doping of the pure boron cluster with an M atom. The embedding energy on the other hand is defined as the gain in energy due to the embedding of an M atom in the tubular shaped pure boron cluster (obtained from the structure of the doped cluster by removing the M atom and optimization). These results are given in Table 1.

Table 1. The binding energy, embedding energy, and doping energy for $M@B_{14}$ (M = 3*d* atom) clusters in the lowest energy configuration as obtained from VASP calculations using GGA. For reference, the binding energy of the B_{14} cluster in the lowest energy configuration is 5.29 eV/atom.

$M@B_{14}$	Binding energy (eV/atom)	Doping energy (eV)	Embedding energy (eV)	HOMO-LUMO gap (eV)
Sc	5.06	1.83	5.91	0.34
Ti	5.16	3.29	6.41	0.15
V	5.24	4.51	6.87	0.27
Cr	5.23	4.38	6.41	1.31
Mn	5.26	4.77	6.78	0.57

Fe	5.38	6.65	9.87	1.30
Co	5.39	6.77	8.85	0.32
Ni	5.30	5.43	7.45	1.73

The doping energies for $Fe@B_{14}$, $Co@B_{14}$, and $Ni@B_{14}$ are larger than their respective binding energies which in turn are higher compared with the binding energy of the lowest energy isomer of pure B_{14} cluster. This indicates that *these doped clusters are energetically more favorable compared with the lowest energy isomer of the undoped boron cluster*. Some of the 3*d* TM atom doped drum-shaped boron structures show high HOMO-LUMO gap such as $Cr@B_{14}$ (1.31 eV), $Fe@B_{14}$ (1.30 eV), and $Ni@B_{14}$ (1.73 eV) and zero magnetic moment. These values are obtained using GGA in VASP and the actual values are likely to be significantly higher. In the case of $Co@B_{14}$ the HOMO-LUMO gap is 0.32 eV, which is small due to the odd number of electrons. In fact, $Co@B_{14}$ anion is isoelectronic to $Ni@B_{14}$ and has a large HOMO-LUMO gap of 1.81 eV which is comparable to that of $Ni@B_{14}$. $Co@B_{14}^{+}$ is isoelectronic with $Fe@B_{14}$ and it also has a large HOMO-LUMO gap of 1.53eV which is comparable to that of $Fe@B_{14}$. In the following we present some details of the atomic structure and our analysis of the distribution of electrons in each of these cases in order to understand their stability.

In general, the B-B bond length within each B_7 ring of the drum-shaped structure is smaller compared with the B-B bond length between the rings. For M = Ni, both the boron rings are identical and the B-B bond length is 1.63 Å, but for Fe, the B-B bond length in one ring is shorter (1.61 Å) than in the other ring (1.67 Å), though there is 7-fold rotational symmetry. The inter-ring

B-B bond length is longer, with the value of 1.87 Å for M = Ni and 1.79 Å for M = Fe. The B-Ni bond length is 2.05 Å, while for B-Fe, there are two bond lengths (1.99 Å with the B atoms in the smaller ring and 2.13 Å for the B atoms in the other ring). The structure of the drum shows similarity in cases where the number of valence electrons is the same, such as for $Co@B_{14}^-$ anion and neutral $Ni@B_{14}$; $Co@B_{14}^+$ cation, neutral $Fe@B_{14}$, and $Mn@B_{14}^-$ anion; as well as $Mn@B_{14}^+$ cation and neutral $Cr@B_{14}$ (see Fig. 1 for the atomic structures of the neutral clusters).

The drum-shaped boron clusters doped with a TM atom exhibit covalent bonding between boron atoms as well as delocalized charge that plays an important role in understanding the stability of the doped clusters. We use a jellium model to represent the delocalized charge and to understand the stability due to hybridization of the molecular orbitals of the boron drum with the valence orbitals of the M atom such as in $Ni@B_{14}$. A disk jellium model represents well the drum structure of these clusters and has been successfully used recently[18] to explain the stability of doped quasi-planar boron clusters, especially B_7P and B_8Si. According to this model, clusters with 12 delocalized valence electrons are magic and this results in their high stability. Further magic clusters arise for disc-shaped jellium clusters with 24 valence electrons. This is the case of $Ni@B_{14}$ which has 24 (delocalized) valence electrons. This is well suited to a disk jellium model to make it a magic cluster, as is also evident from its large HOMO-LUMO gap. Within PBE0/6-311+G level of theory in Gaussian09, the HOMO-LUMO gaps for $Fe@B_{14}$ and $Ni@B_{14}$ clusters are 3.03 eV and 3.18 eV, respectively. These large values suggest high chemical stability of these species. One can have 24 (delocalized) valence electron clusters for $M@B_{16}$ drum structure such as M = Fe neutral and $Mn@B_{16}^-$ anion as well as $Co@B_{16}^+$cation. We shall discuss such clusters later.

3.2 Electronic Structure and Stability of Drum-Shaped $M@B_{14}$ Magic Clusters. Some of the molecular orbitals of $Ni@B_{14}$ and their energies, as obtained from the Gaussian09 calculations

with PBE0 functional, are shown in Fig. 2, along with those of the B_{14} drum without the Ni atom. An analysis of the molecular orbitals and energy levels shows that there are seven occupied π bonded delocalized molecular orbitals of the B_{14} drum structure that account for 14 valence electrons of the boron framework. These molecular orbitals are of d_z2, s, p_x, p_y, $f_{yz}2\text{-}_{yr}2$, $f_{xz}2\text{-}_{3xr}2$, and p_z type. Accordingly, each boron atom contributes two electrons to the two-center and three-center σ bonded tubular framework of B_{14}. The 14 delocalized electrons and 10 valence electrons of nickel atom give a total count of 24 valence electrons, which corresponds to a magic number in a disc jellium model. One can see that after hybridization with Ni orbitals, 5 *d* type orbitals are occupied and another *s* type orbital of the cage becomes occupied. The HOMO in both the B_{14} and Ni@B_{14} cases remains of p_z type. The LUMO of the Ni@B_{14} cluster is a *g* type molecular orbital and there is a large HOMO-LUMO gap. The *f* type molecular orbitals in the B_{14} and Ni@B_{14} cases remain at nearly the same energy positions, suggesting little participation in the hybridization with Ni orbitals. The high chemical stability for Co@B_{14} anion can again be attributed to 24 valence electrons in a disk jellium model. The positions of the *f* orbitals for M = Fe are slightly changed because of the deformation of the drum structure, as the Fe atom moves towards one of the rings and the two B_7 rings are not identical. This lowers the symmetry and leads to some deformation in the molecular orbitals, as shown in Fig. 2. In this case the second s type molecular orbital is unoccupied. Also, the d_{yz} and d_{zx} type hybridized orbitals are unoccupied while two more *f* type molecular orbitals of the drum get occupied. Therefore, the stability of the Fe doped B_{14} drum structure is related to the presence of 22 (delocalized) valence electrons.

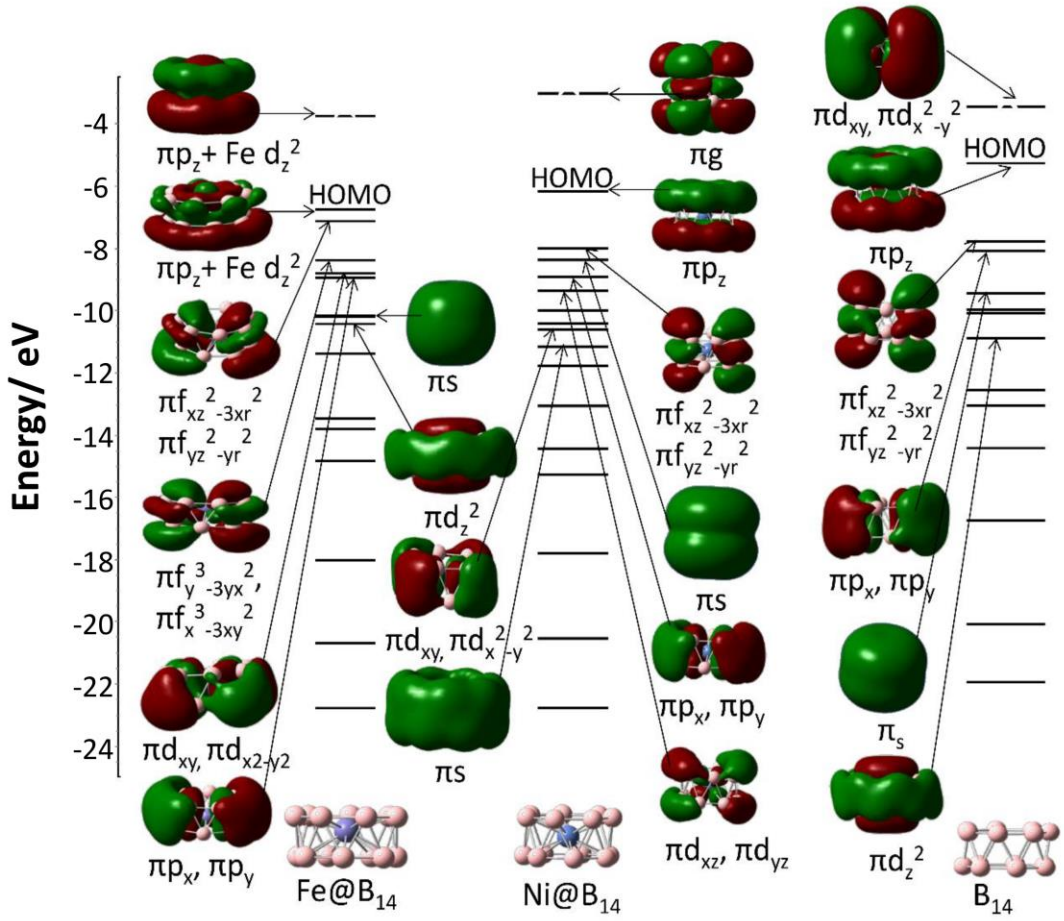

Figure 2. The molecular orbitals of drum-shaped neutral Fe@B_{14} and Ni@B_{14} clusters, as well as those of the pure B_{14} symmetric drum-shaped cluster without Ni atom. The different π-bonded molecular orbitals involved in the bonding are also shown. Note that the Fe atom is displaced towards one of the boron rings, which becomes slightly smaller than the other ring. The dashed lines show the LUMO.

3.3 Bonding Characteristics in Drum-Shaped M@B_{14} Structures. In order to understand the electronic stability and bonding characteristic of the drum-shaped M doped B_{14} clusters, we studied ELF of the doped and the undoped drum-shaped B_{14} structures and further analyzed the electronic

charge density. ELF isosurface at 0.8 shows (Fig. 3) localization of the electron density on two-centered bonds of the B_7 rings. Further, ELF analysis of B_{14} structure at isovalue 0.7 (Fig. 3) also indicates the presence of three-centered σ bonded framework of the drum. This picture is consistent with AIMAll analysis of the doped systems as discussed below.

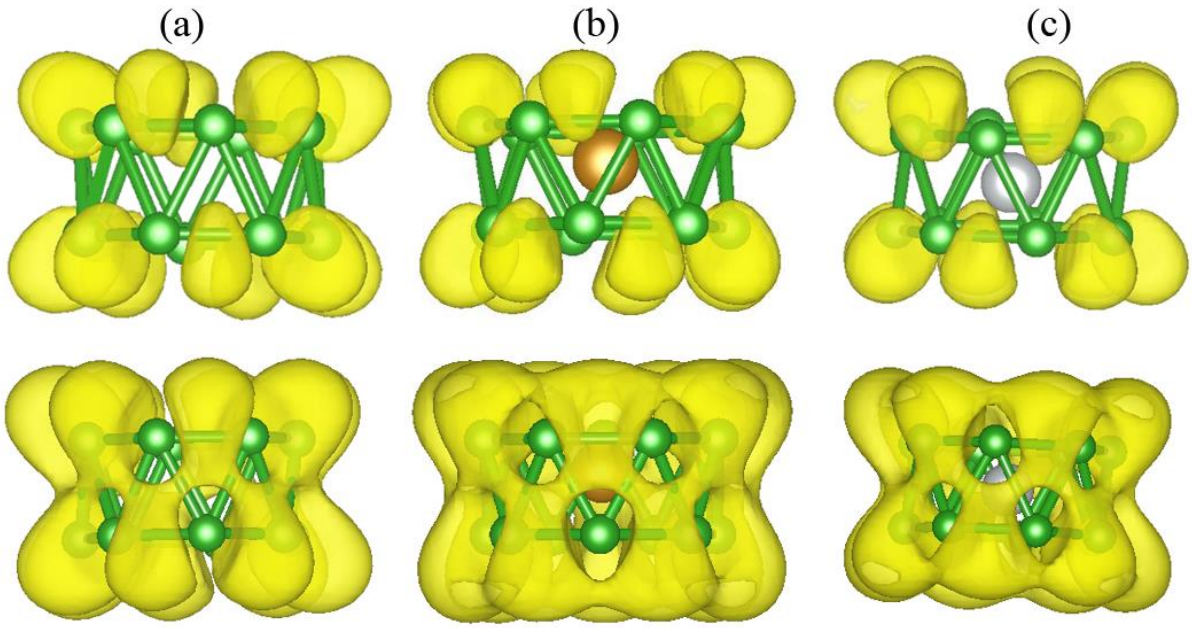

Figure 3. (Upper panel) Isosurfaces (isovalue 0.8) and lower panel (isovalue 0.7) of ELF for (a) B_{14} drum structure, (b) Fe@B_{14}, and (c) Ni@B_{14}, respectively. 2-center σ bonding is seen in B_7 rings, while 3-center σ bonding is seen in boron framework in all the three cases.

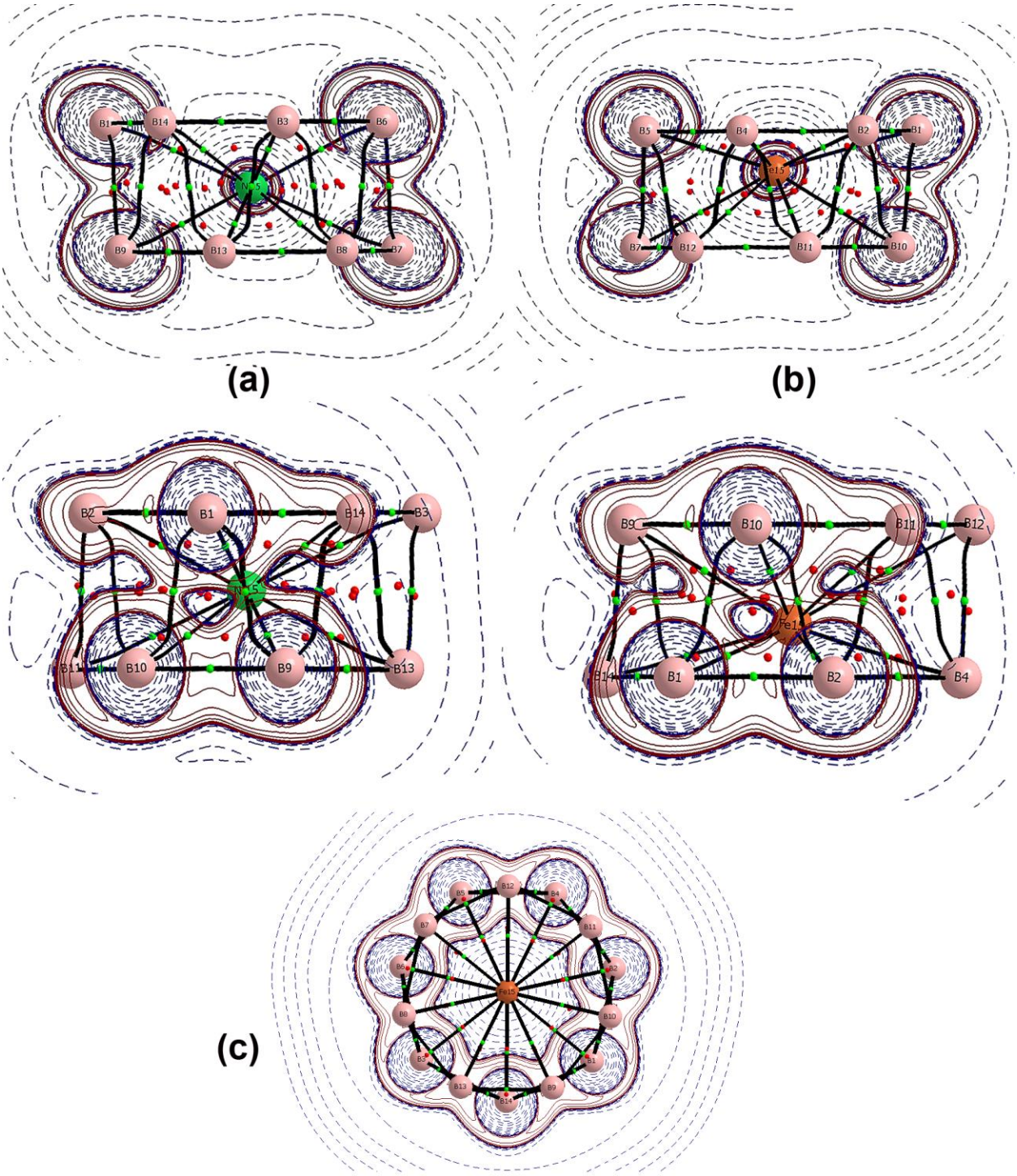

Figure 4. Contours of the Laplacian of the electron density for (a) Ni@B_{14} and (b) Fe@B_{14} drum-shaped structures. The top row shows contours in a plane passing through four boron atoms at opposite ends of the drums, and the metal atom, while the bottom row shows contours in a plane

passing through three adjacent boron atoms, one on the top face and two on the bottom face of the drum. (c) Contours of the Laplacian of the electron density for Fe@B_{14} drum-shaped structure in a plane passing through one of the drum faces (B_7 ring). Full (dashed) line contours show charge accumulation (depletion). Accumulation of charge is seen in B_7 rings. BCPs are shown as green dots and RCPs as red dots. Bond paths are shown with a full line. Pink balls show B atoms while the large green and orange balls show Ni and Fe atoms, respectively.

Figure 4 shows contours of the Laplacian of the electron density, as well as the bond paths, BCPs and RCPs obtained from AIMAll calculations. Analysis of the Laplacian of the electron density indicates prevalence of two center and three center bonding in the boron drum structure, and extensive delocalization of electron density of the boron drum over the M atom. Molecular orbital pictures provide more detailed insight of the behavior of the 14-valence electrons and their delocalization. As discussed above, analysis of the molecular orbitals reveals that these seven π-bonded molecular orbitals of the undoped B_{14} disc-shaped cluster are of the *s*, p_x, p_y, p_z, d_z^2, $f_{xz^2-3xr^2}$ and $f_{yz^2-yr^2}$ type, as shown in Fig. 2. The π molecular orbitals of the boron cage hybridize with the 3*d*, 4*s*, and 4*p* orbitals of the 3*d* TM atom. In the case of Ni@B_{14}, the doping of nickel atom in B_{14} cluster gives rise to twelve such hybridized molecular orbitals which are of the types *s*, p_x, p_y, p_z, d_z^2, $d_{x^2-y^2}$, d_{xy}, d_{xz}, d_{yz}, *s*, $f_{yz^2-yr^2}$and $f_{xz^2-3xr^2}$. These twelve molecular orbitals accounting for 24 valence electrons, and the σ bonded orbitals of the boron drum, give rise to the chemical stability of Ni@B_{14}. Fe@B_{14} also shows high chemical stability with a GGA HOMO-LUMO gap of 1.30 eV. There are 22 electrons which reside in the delocalized π bonded molecular orbitals of the B drum and the valence orbitals of the Fe atom, while the rest of the valence electrons occupy the σ-bonded framework. These 22 electrons reside in the *s*, p_x, p_y, p_z, d_z^2, d_{xy}, $d_{x^2-y^2}$, $f_{xz^2-3xr^2}$, $f_{yz^2-yr^2}$, f_{y^3-}

$_{3yx}^2$, f_x^3-$_{3xy}^2$ type orbitals with hybridization of Fe atomic orbitals. The second *s* type molecular orbital in Fe@B_{14} is not occupied, in contrast to the Ni case; two *d* type molecular orbitals are unoccupied, while two more *f* type molecular orbitals become occupied. Therefore, the electronic structure of the Fe doped drum is different from that of the Ni doped drum. The HOMO-LUMO gap is lower than in Ni@B_{14}. However, the Co@B_{14} anion cluster also attains a 24-valence electron configuration. It has a large HOMO-LUMO gap of 1.81 eV as compared to its cationic form Co@B_{14}^+, which has a HOMO-LUMO gap of 1.53 eV; the latter is also deformed as in the case of Fe doping.

AIMAll analysis of the doped boron and drum-shaped B_{14} clusters reveals their bonding characteristics. There are three types of bonds: two-centered bonds between the nearest neighbor atoms of each B_7 ring, whilst three-centered bonds connect the boron atoms of the two rings, and lastly there are metal-boron bonds. We analyzed the Laplacian distribution, $L(\mathbf{r}) = -¼\nabla^2\rho(\mathbf{r})$, as well as the BCPs and RCPs of the charge density. Electron density is accumulated in regions with $L(\mathbf{r}) > 0$, while regions with $L(\mathbf{r}) < 0$ correspond to electron depletion. These are shown in Figs. 4 and 5. The Laplacian distribution at the BCPs of the two-centered bond in the B_7 rings shows a large positive value (0.06 e/bohr^6 in the case of Ni@B_{14},) indicating strong covalent bonding. Laplacian distribution at BCPs of three-centered bonds interconnecting B_7 rings have a lower Laplacian value of around 0.01 e/bohr^6. Since these are three-centered bonds, an increase in the delocalization of the electron density is expected. Even in the ELF analysis, the three-centered bonds are observed at a lower isosurface value of 0.7. The Laplacian at BCPs of nickel-boron bonds lies in the range of -0.02 to -0.03 e/bohr^6. The negative $L(\mathbf{r})$ indicates electron depletion and coordinate bonding. These results of Laplacian of the electron density for M doped clusters are

similar to those for B_{14} drum-shaped cluster obtained by removing the M atom (without reoptimization), shown in Fig. S1 in Supplementary Information.

The structure of $Fe@B_{14}$ is not symmetric, as the iron atom is not present at the center of the drum but is closer to one of the B_7 rings, which has slightly shorter B-B bonds than in the other B_7 ring. This asymmetry is also observed in the case of $Co@B_{14}^+$. This doped cation cluster is isoelectronic to $Fe@B_{14}$ and its atomic structure is also similar to that of $Fe@B_{14}$. In these cases, there are five different types of bonds: two types of two-centered boron-boron bonds in the two B_7 rings, three-centered bonds along the rim of the boron drum connecting different B_7 rings, and two types of M-boron bonds (proximal B_7 ring-M bonds and distal B_7 ring-M bonds). The Laplacian at the BCPs of the two-centered bonds in the distal B_7 ring is around 0.06 e/bohr^6 similar to the Ni doped case, while the Laplacian at the BCPs of the proximal B_7 ring bonds is lower (around 0.04 e/bohr^6). The decrease in the value of Laplacian at these BCPs can be explained by the fact that the electron density of the proximal B_7 ring interacts more strongly with the iron atom. This weakens the extent of localization of the two-centered bonds in the proximal B_7 ring. The Laplacian at the BCPs of the M atom to the proximal B_7 ring is -0.02 e/bohr^6 while that for the distal B_7 ring is -0.04 e/bohr^6. This indicates that the iron atom interacts more strongly with the proximal B_7 ring than with the distal ring. Figure 5(c) shows the bond ellipticity. As expected the bond ellipticity is close to zero for the B-B bonds in the B7 rings due to strong covalent bonding, while the bond ellipticity increases significantly for the inter-ring bonds as well as M-B bonds, due to reduced covalency in these bonds. The Laplacian for all RCPs is negative, as shown in Fig. 5(d) for $Ni@B_{14}$.

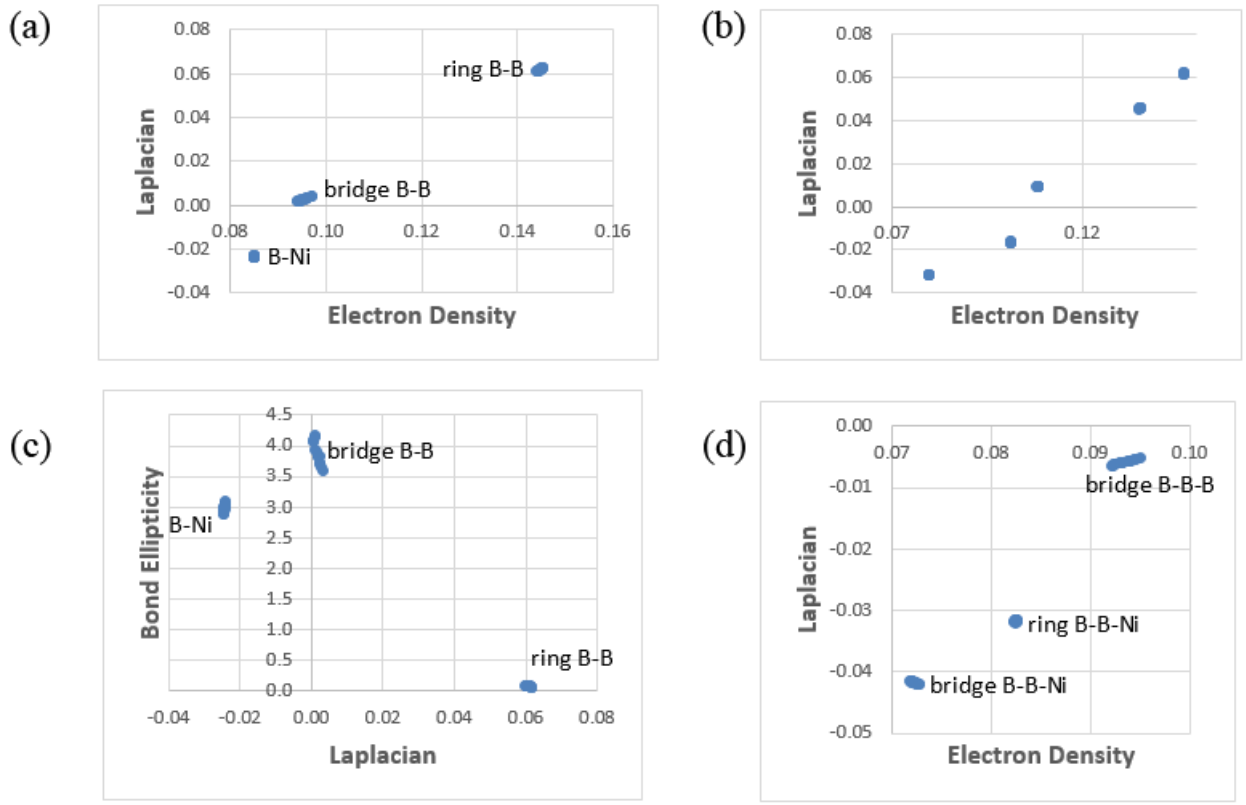

Figure 5. Laplacian vs electron density distribution at BCPs of various bonds in (a) Ni@B_{14} and (b) Fe@B_{14}, showing the clustering of BCPs by type. (c) Bond ellipticity vs Laplacian at BCPs and (d) Laplacian vs electron density distribution at RCPs in Ni@B_{14}.

Table 2. Atomic source function contributions to the electron densities at representative BCPs for each type of bond in $Ni@B_{14}$ and $Co@B_{14}$.

BCP	Bonded atoms		Nearest neighbors		Other atoms	
	$B_{14}Co$	$B_{14}Ni$	$B_{14}Co$	$B_{14}Ni$	$B_{14}Co$	$B_{14}Ni$
B1 B2 (ring)	71.60%	73.56%	19.15%	16.52%	9.25%	9.93%
B1 B9 (bridge)	48.81%	46.71%	34.45%	35.41%	16.74%	17.88%
B1 M	29.66%	29.36%	37.33%	37.09%	32.95%	33.56%

We have also analyzed the source function at the BCPs of the different bonds in $Fe@B_{14}$, $Co@B_{14}$ and $Ni@B_{14}$. The values of the atomic source function are shown in Table 2. B1 and B2 (here the number indicates the atom number) are adjacent atoms in a B_7 ring of $Ni@B_{14}$ which are involved in a two-centered bond. The bond is a strongly covalent bond, as the source function analysis reveals that the electron density at the BCP between B1 and B2 arises primarily from contribution of the bonded atoms. This is in contrast to the BCP between B1 and B9. These atoms are in different B_7 rings of $Ni@B_{14}$, and are connected to each other via three-centered bonding. The contributions of these atoms to the electron density at the BCP is lower, indicating the presence of delocalization, as expected of three-centered bonding. The difference between these two kinds of boron-boron bonds is also evident from the Laplacian distributions in Figs. 4 and 5. The contribution of the bonded atoms to the electron density at the BCP of a metal-boron bond is very low, pointing to extensive conjugation. This supports the jellium model used here to understand the stability, as well as agrees with the bond ellipticities. The delocalized electron cloud of the M atom interacts with that of the boron drum to give a stable electronic configuration. A similar trend

is observed in a comparison of the atomic source function contributions to the electron densities at the corresponding RCPs (Table 3). One can see a reduction in the value for the ring atoms as compared to the BCPs in Table 2.

Table 3. Atomic source function contributions to the electron densities at representative RCPs for each type of bond in Ni@B_{14} and Co@B_{14}.

RCP	Ring atoms		Nearest neighbors		Other atoms	
	$B_{14}Co$	$B_{14}Ni$	$B_{14}Co$	$B_{14}Ni$	$B_{14}Co$	$B_{14}Ni$
B1 B2 M (ring)	40.60%	41.15%	36.35%	35.31%	23.00%	23.41%
B1 B2 B10	61.00%	59.00%	25.13%	26.19%	13.86%	14.82%
B1 B10 M (bridge)	28.73%	25.90%	40.79%	42.05%	30.43 %	32.11 %

A similar scenario is observed for Fe@B_{14} (Table 4), except for the fact that as mentioned earlier, there are five types of bonds in Fe@B_{14} (unlike the case of Ni@B_{14}), due to the presence of asymmetry in the atomic structure. The BCPs between B2 and B1, and between B7 and B8 atoms of the other B_7 ring, again represent two-centered bonding inside the B_7 rings of the drum structure, deriving the major share of their electron densities from the respective bonded atoms. In contrast, the BCP between the B8 and B6 atoms, which are from different B_7 rings, derives a much lower contribution of its electron density from the bonded atoms, and is part of a three-centered bond.

Table 4. Atomic source function contributions to the electron densities at representative BCPs for each type of bond in $Fe@B_{14}$.

BCP	Bonded atoms	Nearest neighbors	Other atoms
B2 B1 (proximal ring)	68.35%	21.75%	9.85%
B8 B6 (bridge)	49.80%	34.00%	16.14%
B7 B8 (distal ring)	72.06%	18.88%	9.00%
B2 (proximal ring) Fe15	38.80%	33.15%	28.01%
B12 (distal ring) Fe15	20.64%	41.50 %	37.84%

Analysis of LDM (Tables S6-S8 in Supplementary Information) in $Fe@B_{14}$, $Co@B_{14}$, and $Ni@B_{14}$ shows that in all three clusters, approximately 3.15 electrons are localized in the basin of each boron atom, and approximately 1.46 electrons are shared between each boron atom and neighboring boron atoms. Bonds connecting neighboring boron atoms in a ring, *e.g.* B1-B2 and B1-B14, share almost twice the electron density (0.92 electrons in $Fe@B_{14}$, 0.96 in $Co@B_{14}$ and 1.0 in $Ni@B_{14}$) as do bonds connecting neighboring boron atoms in different rings, *e.g.* B1-B9 and B1-B10 (0.52 electrons in $Fe@B_{14}$, 0.5 in $Co@B_{14}$ and 0.44 in $Ni@B_{14}$). This supports the interpretation of covalent bonding between neighboring boron atoms in each B_7 ring, versus three-center bonding in the 14 B-B-B triangles connecting the two rings.

It is worth pointing out that the number of electrons localized on an atom or delocalized between a pair of atoms as determined by LDM may be different from that given by orbital models, where

the electrons localized on an atom are just the core and non-bonding electrons (two for boron). In LDM these numbers are computed from the double integrations over atomic basins in equations (7) - (10), and do not assume any core-valence separation. The atomic localization indices (~3.15 electrons) for $M@B_{14}$ clusters are comparable to those obtained for pure boron ring clusters (B_n in the range n = 3-10) studied by us earlier[18]. The delocalization indices for BB bonds in the B_7 rings are comparable to but somewhat smaller than the peripheral bonds[18] in pure B_n ring clusters (n = 3-10), indicating that the BB bonds in the B_7 rings of $M@B_{14}$ clusters are not as covalent as in the pure B_n ring clusters. Likewise, bonds with high ellipticities (see Fig. 5c) between boron atoms in different B_7 rings have delocalization indices comparable to but on the lower range of the values for similar high ellipticity "radial" bonds between the central atom and the ring atoms of pure B_n ring clusters. Note that for strongly directional covalent bonds the ellipticity will be zero.

3.4 Vibrational Spectra of Drum-Shaped $M@B_{14}$ Clusters. We further calculated the vibrational spectra of neutral and cation $Fe@B_{14}$, $Co@B_{14}$, and $Ni@B_{14}$ drum-shaped structures using Gaussian09 with PBE0 functional and found all the frequencies to be real. This suggests dynamical stability of these structures. The IR absorption spectra are shown in Figs. 6 and 7 for cation and neutral Fe, Co, and Ni doped boron clusters, respectively, while the IR intensities and Raman activities are tabulated in Table S9 in Supplementary Information. The lowest vibrational mode for each of them consisted of the M atom moving out of the plane of the boron drum in the z direction (taken to be perpendicular to the B_7 rings). The frequency of this mode for Fe, Co, and Ni doped neutral clusters is 398 cm^{-1}, 149 cm^{-1}, and 302.5 cm^{-1}, respectively. The low frequency mode corresponds to weaker bonding between the M atom and the boron drum compared to that between boron atoms. For neutral $Fe@B_{14}$, the dominant modes are at 543 cm^{-1} (scissor mode, doubly degenerate), and two breathing modes at 769 cm^{-1} and 802 cm^{-1}. For neutral $Co@B_{14}$, the

dominant modes are at 511 cm^{-1} (scissoring mode), 535 cm^{-1} (bending mode), and 880 cm^{-1} (stretching and bending mode). These are all doubly degenerate. For neutral $Ni@B_{14}$, the doubly degenerate dominant modes are at 407 cm^{-1} (scissoring mode), 518 cm^{-1} (bending mode), and 880.5 cm^{-1} (stretching and bending mode). The vibrational frequency having the highest intensity involves scissor movement of the boron rings, while the M atom oscillates around its position in the xy plane. The highest frequency vibrational mode of these clusters consists of asymmetrical stretching in the two B_7 rings coupled with slight oscillation of the M atom in the xy plane. The frequency of this vibrational mode is nearly independent of the M atom. In the case of cations of M = Fe and Ni, this mode is doubly degenerate. For the case of Fe doping, the dominant modes are: stretching and bending mode at around 885 cm^{-1}, breathing mode at 743.7 cm^{-1}, doubly degenerate scissoring mode at around 585 cm^{-1}, doubly degenerate scissoring-bending-stretching mode at around 516 cm^{-1}, and a breathing mode at 267 cm^{-1}, but for the case of Co cation, the highest frequency mode splits as the two B_7 rings are different and occurs at 889 $cm^{-1}$and 871.5 cm^{-1} (both doubly degenerate). The other modes are at 728 cm^{-1} (breathing, single mode), doubly degenerate scissoring mode at 597 cm^{-1}, scissor modes at 551 cm^{-1} and 553 cm^{-1}, a doubly degenerate bending-stretching mode at 506.5 cm^{-1}, and a bending mode at 260 cm^{-1}. For Ni doped cation cluster, the modes are: doubly degenerate stretching mode at 869 cm^{-1}, breathing mode at 738 cm^{-1}, doubly degenerate scissor mode at 510 cm^{-1}, scissor modes at 500 and 503 cm^{-1}, and a breathing-bending mode at 202 cm^{-1}. We also calculated Raman spectra of cation as well as neutral clusters with M = Fe, Co, and Ni, and these are given in Figs. S2 and S3 in Supplemental Information.

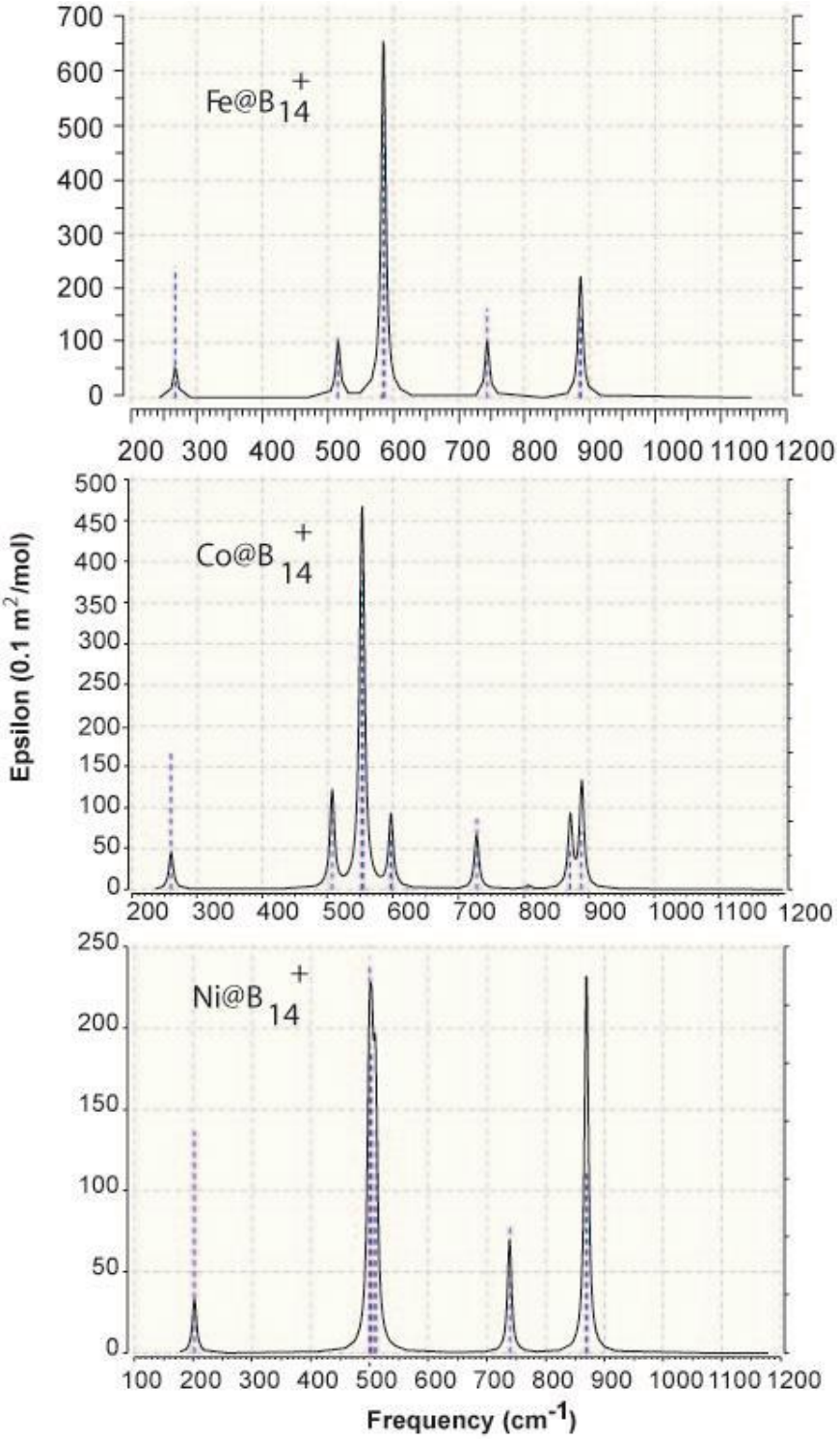

Figure 6. The IR absorption coefficient of $M@B_{14}^{+}$ (M = Fe, Co, and Ni) cation clusters.

The IR intensities are given in Supplementary Information.

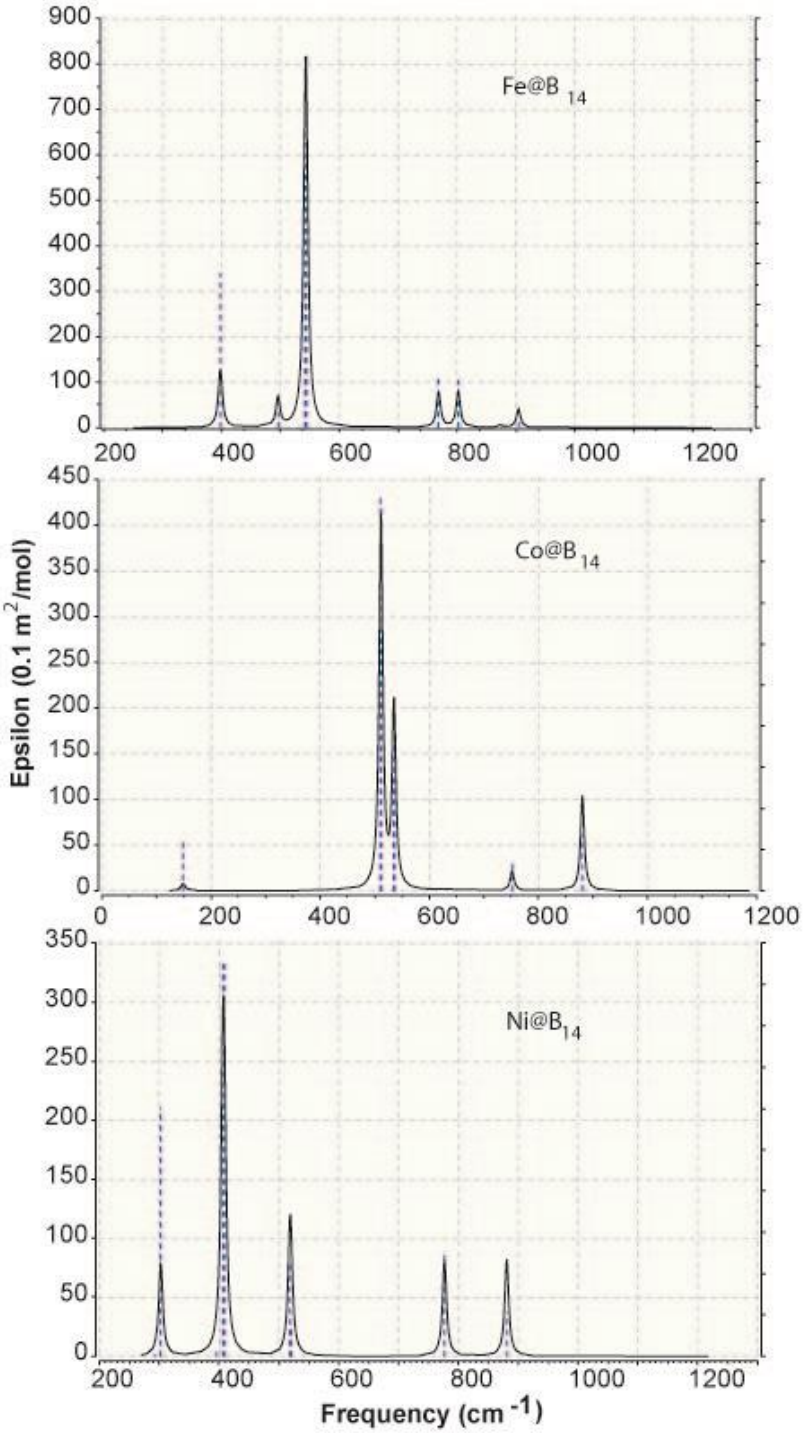

Figure 7. The IR absorption coefficient of M@B_{14} (M = Fe, Co, and Ni) neutral clusters. The IR intensities are given in Supplementary Information.

3.5 Ionization Potential, Detachment Energies, and Electronic Density of States. The vertical detachment energy (VDE) and adiabatic detachment energy (ADE) of the $Ni@B_{14}$ neutral cluster are particularly low, as shown in Table 5, suggesting that this structure has high stability. The ionization potentials (IPs) are also given in Table 5. IPs of $Fe@B_{14}$ and $Ni@B_{14}$ clusters are relatively large, which is also indicative of their stability. In the case of $Co@B_{14}$, the VDE and ADE are larger, while the IP is smaller than the values for the Ni and Fe doped systems. This is due to the fact that neutral $Co@B_{14}$ is not a closed shell system because of the odd number of electrons.

Table 5. Vertical detachment energy (VDE), adiabatic detachment energy (ADE) and ionization potential (IP) of selected doped clusters.

Cluster	VDE(eV)	ADE (eV)	IP (eV)
$Fe@B_{14}$	3.08	3.37	6.48
$Co@B_{14}$	3.39	3.61	6.11
$Ni@B_{14}$	2.28	2.33	6.43

The Gaussian broadened electronic densities of states of $M@B_{14}$ (M = Fe, Co, and Ni) anion clusters are shown in Fig. 8. These results may be compared with photoelectron spectroscopy data when it becomes available. This as well as the IR and Raman data will help to establish the atomic structures of these clusters. As expected the HOMO-LUMO gap for M = Co is large as it is a closed shell system, while for Ni it becomes quite small as there is an odd number of electrons

which is one electron more than the electronic closed shell structure. The calculations in this case were done with spin polarization. In the case of Fe also the number of electrons is odd and the HOMO-LUMO gap is intermediate.

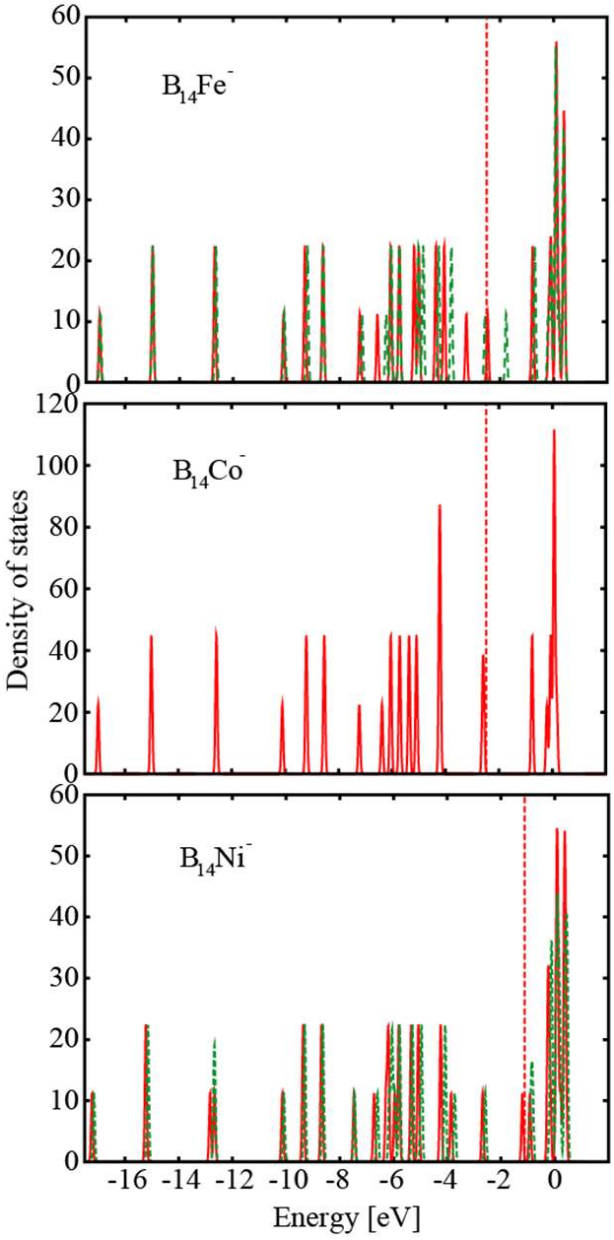

Figure 8. Gaussian broadened electronic density of states of the anion $M@B_{14}$ clusters (M = Fe, Co, and Ni). The vertical broken line shows the HOMO. In the case of Fe and Ni, the calculations were done with spin polarization, but the exchange-splitting is small.

3.6 Stability of Drum-Shaped $M@B_{16}$ (M = Mn, Fe, and Co) Clusters

Recently anions of $M@B_{16}$ (M = Mn and Co) have been obtained[12,13] in experiments and a drum-shaped structure has been reported. From our analysis of the stability of $M@B_{14}$ clusters with 24 (delocalized) valence electrons, we anticipate that anion of $Mn@B_{16}$, neutral of $Fe@B_{16}$, and cation of $Co@B_{16}$ could also be magic with 24 delocalized valence electrons (assuming one electron from each B atom contributing to the delocalized charge), though the size of the two B_8 rings increases compared to the case of M doped B_{14} clusters, and that could make M-B interactions weaker. Accordingly, we performed calculations on neutral, cation, and anion of these clusters, as well as other similar systems to understand their stability. These calculations were performed with spin polarization using both VASP as well as Gaussian09 programs. The atomic structures of the clusters with 24 delocalized valence electrons are shown in Fig. 9, while for other clusters the atomic structures are shown in Fig. 10. It is found that for neutral $Fe@B_{16}$ and cation of $Co@B_{16}$ (both with C_2 symmetry), a singlet state of the drum structure is favored while for the anion of $Mn@B_{16}$ (C_4v symmetry), a triplet state of the drum structure is 0.39 eV lower in energy than a singlet state. The GGA HOMO-LUMO gap for $Co@B_{16}$ cation is relatively large (0.86 eV) which supports the special stability at 24 delocalized valence electrons, but for the Fe doped neutral cluster and anion of Mn doped cluster, the GGA value of the HOMO-LUMO gap is 0.41 eV and 0.32 eV, respectively. In these two cases, the Mn and Fe atoms are slightly displaced from the

center as we also obtained for $Fe@B_{14}$ cluster. Accordingly, the behavior of Mn and Fe doped clusters is different from that of the Co doped cluster. The triplet state of $Mn@B_{16}$ anion cluster suggests two unpaired electrons. Accordingly, we studied a cation of $Mn@B_{16}$ and $Cr@B_{16}$. For $Mn@B_{16}$ cluster a triplet state is again lower in energy than a singlet state, but for $Cr@B_{16}$, a singlet state is favored and the GGA HOMO-LUMO gap is relatively large (0.82 eV), again suggesting special stability of this cluster similar to $Fe@B_{14}$, corresponding to 22 delocalized valence electrons.

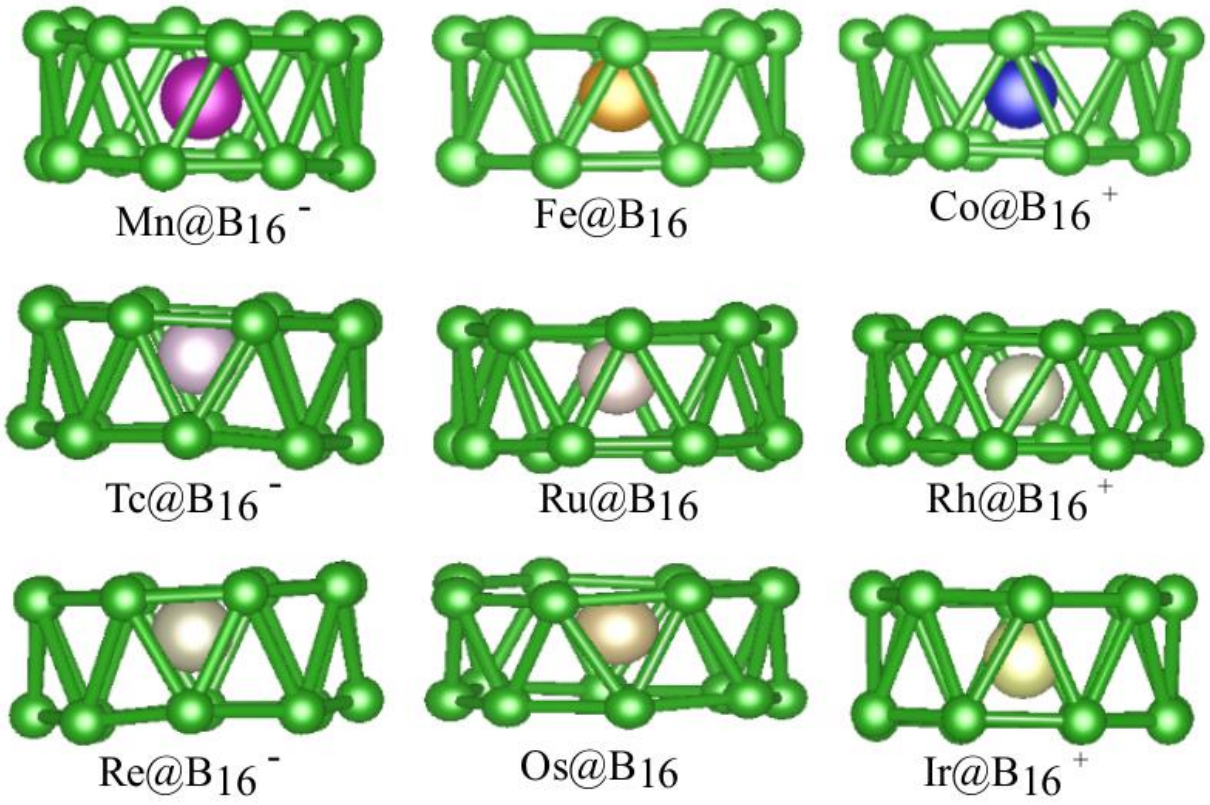

Fig. 9. Optimized atomic structures of drum-shaped $M@B_{16}$ clusters with 24 delocalized valence electrons as obtained from VASP calculation. The GGA HOMO-LUMO gaps (multiplicity) are 0.32 eV (triplet), 0.41 eV (singlet), 0.86 eV (singlet), 0.42 eV (singlet), 0.46 eV (singlet), 0.63 eV

(singlet), 0.48 eV (singlet), 0.46 eV (singlet), 0.65 eV (singlet) for Mn, Fe, Co, Tc, Ru, Rh, Re, Os, and Ir doped clusters, respectively.

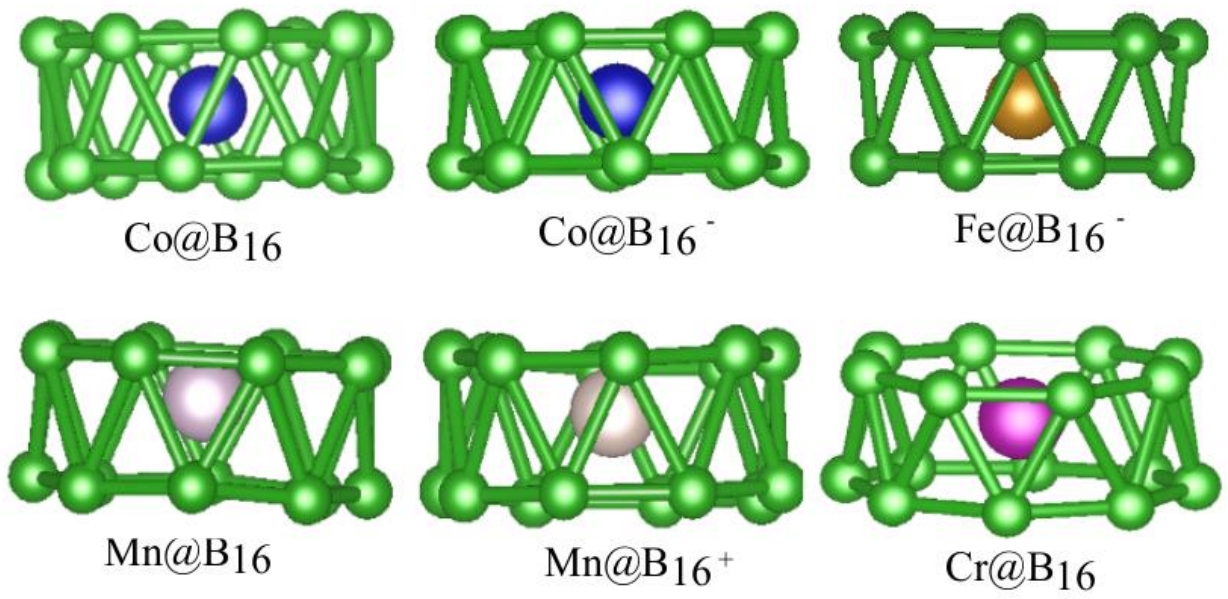

Fig. 10. The optimized atomic structures of $M@B_{16}$ clusters having 22, 23, 25, and 26 delocalized valence electrons as obtained from VASP calculation. The GGA HOMO-LUMO gap (multiplicity) is 0.30 eV (doublet), 0.42 eV (triplet), 0.27 eV (doublet), 0.81 eV (doublet), 0.31 eV (triplet), and 0.82 eV (singlet) for Co doped neutral cluster, Co doped anion cluster, Fe, Mn doped neutral cluster, Mn doped cation cluster, and Cr doped neutral cluster, respectively. Relatively large values for neutral Cr doped cluster corresponding to 22 delocalized valence electrons, and neutral Mn doped B_{16} cluster corresponding to 23 delocalized valence electrons, are notable.

The neutral $Co@B_{16}$ cluster has a doublet state as expected for a system with odd number of electrons, while for the anion of $Co@B_{16}$, interestingly a triplet state with two unpaired electrons

and D_{8d} drum-shaped structure has lower energy than a singlet state. This result is in agreement with the findings of Popov *et al*.[13], and it supports that the shell closer occurs at cation of $Co@B_{16}$ (C_2 symmetry) corresponding to 24 delocalized valence electrons. The GGA value of the HOMO-LUMO gap for neutral $Co@B_{16}$ (C_2 symmetry) and $Co@B_{16}^-$ (D_{8d} symmetry) anion (both with open shell structure) is 0.30 eV and 0.42 eV, respectively, values much smaller than for the cation cluster. There are distortions in the structures of $Fe@B_{16}$ (two B_8 rings have different sizes with average Fe-B bond lengths of 2.208 Å and 2.254 Å, inter-ring B-B bond lengths 1.77-1.81 Å, intra-ring 1.59-1.61 Å) and $Co@B_{16}^+$ (intra-ring bond lengths 1.59-61 Å, and inter-ring B-B bond lengths varying from 1.78 Å to 1.82 Å), both of which have singlet states. This suggests that the M-B bonding may not be optimal in these cases. Further calculations on these systems using PBE0 functional in Gaussian09 code confirmed the same trend of the atomic structures and the energy ordering of the spin isomers, though the value of the HOMO-LUMO gap increased significantly as shown in Table 6. It is found that the PBE0 value of the HOMO-LUMO gap for $Co@B_{16}^+$ cation is 1.94 eV, and for the neutral and anion clusters it is relatively large (~1.7 eV). The VDE of $Co@B_{16}$ is low (2.63 eV), supporting strong stability of the $Co@B_{16}^+$ cation cluster, as we expect from the criterion of 24 delocalized valence electrons. The relatively large value of the HOMO-LUMO gap obtained with PBE0 for the neutral and anion $Co@B_{16}$ clusters suggests also good stability of these radicals and the finding of Co doped anion cluster observed in experiments.[13] Similarly, the anion of Mn doped cluster also has a relatively large HOMO-LUMO gap (1.52 eV) in PBE0, and this also supports the finding of this cluster in experiments.[12] The cation of Fe doped B_{16} cluster has a large HOMO-LUMO gap of 2.13 eV and it is similar to the value for the neutral Mn doped B_{16} cluster, supporting their similar electronic structure with a doublet state. Calculations were also done for Tc, Re, Ru, Os, Rh, and Ir doped drum-shaped clusters. In all these

cases the GGA HOMO-LUMO gap is small as shown in Fig. 9, and the results on other isomers suggest that the drum-shaped isomer are not of the lowest energy in these cases.

Table 6. VDE, ADE, IP, and HOMO-LUMO gap for the neutral and charged $M@B_{16}$ drum-shaped clusters (M = Mn, Fe, and Co).

	VDE (eV)	ADE (eV)	IP (eV)	HOMO-LUMO neutral (eV)	HOMO-LUMO anion (eV)	HOMO-LUMO cation (eV)
$Co@B_{16}$	2.63	2.54	7.02	1.71	1.70	1.94
$Fe@B_{16}$	2.87	2.76	6.51	2.11	1.69	2.13
$Mn@B_{16}$	4.08	2.74	7.52	2.14	1.72	1.52

3.7 Assembly of clusters – The finding of nanotubes of boron with metal doping

The stability of drum shaped clusters makes their assemblies interesting to develop nanotubular structures of boron stabilized by M atoms. To start with, we considered two $M@B_{14}$ (M = Fe, Co, and Ni) clusters placed one over the other to form a dimer along the faces. The optimized structures are shown in Fig. 11. It is found that Fe and Ni doped structures are distorted, while the Co doped dimer retains its structure well. We further stacked one more $M@B_{14}$ cluster to obtain a trimer. The optimized structures (Fig. 11) are again distorted in the cases of Fe and Ni, while the Co doped clusters develop in to a nice tubular structure. Encouraged with this result, we developed an infinite nanotube of Co doped B_{14} clusters and the optimized results are shown in Fig. 12. Interestingly the atomic structure of this boron nanotube is similar as for carbon zig-zag nanotubes with all hexagons of boron and it is stabilized with Co atoms. The bonds in the rings of the drum-shaped clusters become elongated while the inter-ring bonds become shorter (~1.65 Å). The cohesive energy of this nanotube is 5.85 eV/atom which is significantly higher than the value for the drum-

shaped Co@B_{14} cluster. There is 1 μ_B magnetic moment per Co@B_{14} formula unit and the nanotube is metallic. To our knowledge this is the smallest nanotube of boron (diameter of 4.36 Å) with similarity to carbon nanotubes that has been stabilized with the doping of M atoms. Note that unlike carbon a hexagonal layer of boron is not stable and extra boron atoms are needed to fill centers of some hexagons to stabilize an alpha boron layer with some hexagonal holes. Bader charge analysis shows charge transfer from Co to B atoms. The Co-Co bond length is 2.98 Å which suggests significant interactions between Co atoms and the formation of an atomic wire of Co inside the boron nanotube. Further assemblies of Fe@B_{16} drum-shaped clusters leads to another type of boron nanotube with triangular network and Fe atoms inside as shown in Fig. 12. The Fe-Fe bond length is 3.19 Å suggesting weak interaction between Fe atoms. There is 3.36 μ_B magnetic moments per Fe@B_{16} unit in this nanotube and it is also metallic. These nanotubes may have interesting possibilities for interconnects. A detailed account of these results will be published separately.

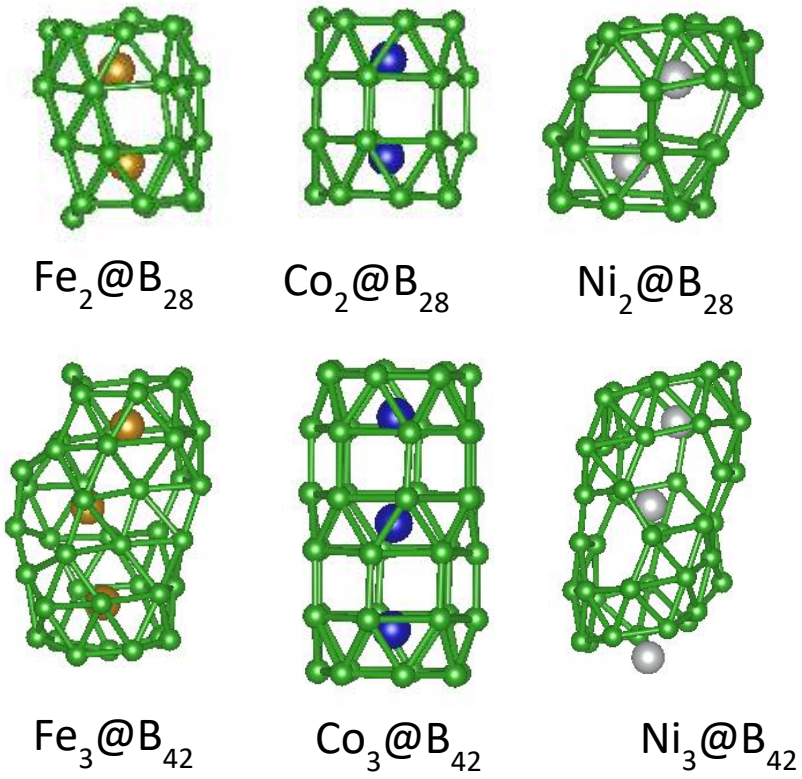

Fig. 11. Stacking of two and three $M@B_{14}$ clusters (M = Fe, Co, and Ni). In the case of Co doping the assembly forms a well ordered finite nanotube.

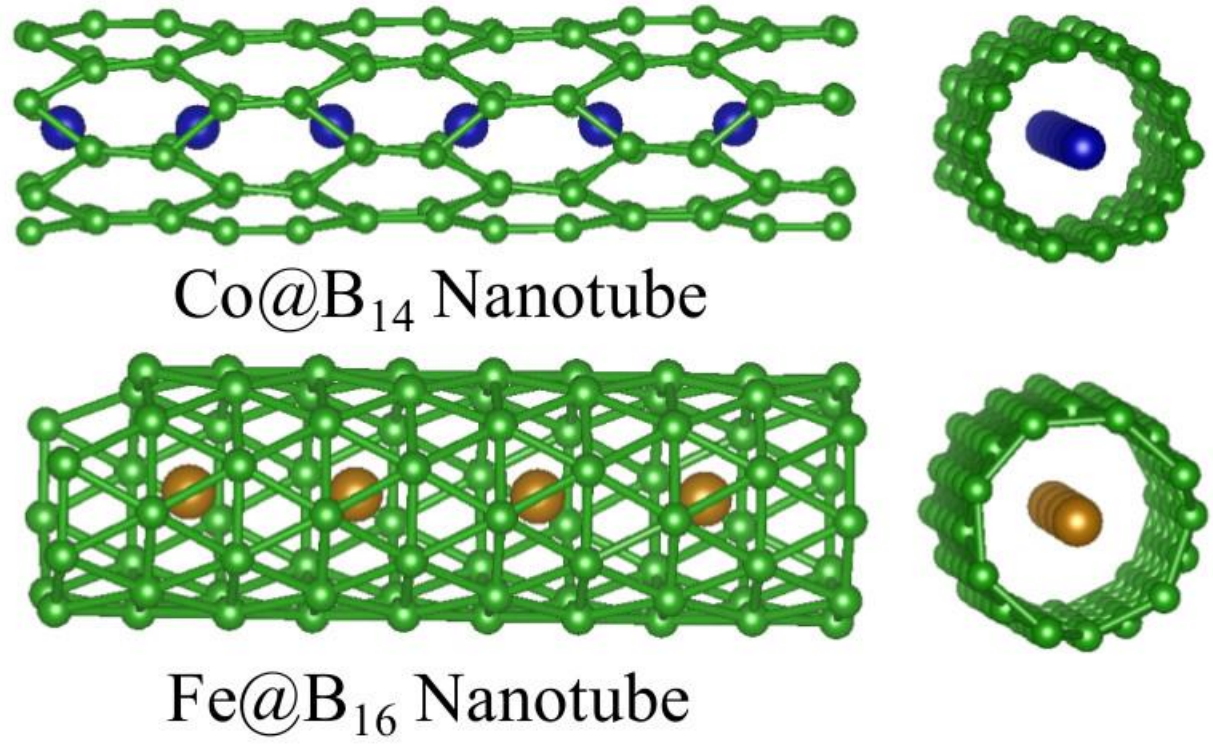

Fig. 12. An assembly of $Co@B_{14}$ clusters to obtain an infinite nanotube of boron stabilized with Co atoms. Both side and cross-sectional views are shown. The B-B bond length in drum-shaped clusters become elongated leading to hexagonal network. The atomic structure of this nanotube has similarity with that of carbon nanotube with all hexagons. Assembly of $Fe@B_{16}$ clusters leads to the formation of another type of boron nanotube with a triangular network.

4. Conclusion

From our analysis of the atomic structure and stability, we have found that the correct size of drum-shaped boron clusters suitable for M atom doping is B_{14}. The correct TM atom for creating highly stable M doped drum clusters is a 3*d* TM atom from Cr to Ni, but Fe, Co, and Ni are special, with large HOMO-LUMO gaps. We find that the drum-shaped isomer is lower in energy than a bowl or conical shaped isomer interacting with M atom, as well as a quasi-planar isomer in which M atom is embedded in the boron network. On the other hand, drum-shaped structure is not favorable for relatively large 3*d* M atoms as well as for 4*d* and 5*d* TM atoms. $Ni@B_{14}$ is a magic TM doped drum-shaped structure. We explained its stability by invoking a 24-electron disk jellium model. $Co@B_{14}^-$ with a large HOMO-LUMO gap of 1.81 eV, is isoelectronic to the 24-electron $Ni@B_{14}$. $Fe@B_{14}$ is also favorable, but the atomic structure is deformed with a lower value of the HOMO-LUMO gap. In order to corroborate our hypothesis, we have analyzed the molecular orbitals of the clusters, and also the electron densities in terms of the Laplacian distributions, critical points, source functions, ELF and electron localization-delocalization indices that support 2-center and 3-center sigma bonding within each ring and between the rings, respectively. The π bonded delocalized charge leads to the stabilization of the drum structure upon interaction with the M atom. These multiple approaches support the view of different types of boron-boron bonds in $M@B_{14}$ clusters – two-centered bonds of essentially covalent character in each B_7 ring, and three-centered bonds with high ellipticity along the rim of the boron drum connecting different B_7 rings. Low electron densities and negative Laplacians characterize the essentially non-covalent M-boron bonding. We have also presented results for the infrared as well as Raman spectra of neutral and cation Fe, Co, and Ni doped clusters, and the electronic densities of states of anion clusters. These can be compared when experimental data becomes available. Further studies have been done on

M doped B_{16} clusters with an emphasis on M = Cr, Mn, Fe, and Co. In particular, it is possible to construct clusters with 22 and 24 delocalized electrons. Our results confirm the earlier finding of $Co@B_{16}$ anion with a triplet state and two unpaired electrons, supporting the applicability of the 24-electron rule to these clusters. In fact, $Co@B_{16}$ cation has a singlet state and a relatively large HOMO-LUMO gap, as also $Fe@B_{16}$ which is also a singlet. There is a subtle change in the atomic structure and associated electronic structure, that leads to the stability of 22 valence electron systems such as for $Cr@B_{16}$. Our results also show stability of open shell systems with relatively large HOMO-LUMO such as for neutral $Mn@B_{16}$. Further we studied assemblies of stable drum shaped $M@B_{14}$ and $Fe@B_{16}$ clusters. We find Co doped $Co@B_{14}$ nanotube of boron that is similar to the carbon nanotube while $Fe@B_{16}$ nanotube has a triangular network of boron atoms. We hope that our findings will encourage experimentalists to look for magic clusters and nanotubes suggested here.

AUTHOR INFORMATION
Corresponding Author
*E-mail: kumar@vkf.in, vijay.kumar@snu.edu.in. Tel/Fax.: +91-124-4079369.
Author Contributions
P. S., V.K., and N.S. contributed equally to this work. A.B.R. performed some of the calculations and contributed to the discussions.
Notes
The authors declare no competing financial interest.

Acknowledgements

We thankfully acknowledge the use of the Magus supercomputing system in SNU. ABR and VK acknowledge support from International Technology Center-Pacific (ITC-PAC). We also thank Dr. Arpan Krishan Deb for preparing some figures.

Supplementary Information

1. Tables S1 gives atomic structures of $B_{10}M$ (M = Fe and W) clusters.

2. Tables S2 gives atomic structures of $B_{12}M$ (M = Fe and W) clusters.
3. Tables S3 gives atomic structures of different isomers of $B_{14}M$ (M = 4*d* element) clusters.
4. Tables S4 gives atomic structures of different isomers of $B_{14}M$ (M = 5*d* element) clusters.
5. Tables S5 gives atomic structures of different isomers of $B_{16}M$ (M = 3*d*, 4*d*, 5*d* element) clusters.
6. Fig. S1 gives the Laplacian for B_{14} drum-shaped cluster.
7. Table S6 gives LDM for $Fe@B_{14}$.
8. Table S7 gives LDM for $Co@B_{14}$.
9. Table S8 gives LDM for $Ni@B_{14}$.
10. Fig. S2 gives Raman activity for cation $M@B_{14}$ (M = Fe, Co, and Ni) clusters.
11. Fig. S3 gives Raman activity for neutral $M@B_{14}$ (M = Fe, Co, and Ni) clusters.
12. Table S9 gives the IR intensities and Raman activities for $M@B_{14}$ clusters.

References

(1) Boustani, I., Systematic Ab Initio Investigation of Bare Boron Clusters: Determination of the Geometry and Electronic Structures of B_n (n = 2–14). *Phys. Rev. B* **1997**, *55*, 16426.

(2) Piazza, Z. A.; Hu, H.S.; Li, W.L.; Zhao, Y.F.; Li, J.; Wang, L.S., Planar Hexagonal B_{36} as a Potential Basis for Extended Single-Atom Layer Boron Sheets. *Nature Commun.* **2014**, *5*.

(3) Zhai, H. J.; Zhao, Y. F.; Li, W. L.; Chen, Q.; Bai, H.; Hu, H. S.; Piazza, Z. A.; Tian, W.J.; Lu, H. G.; Wu, Y.B., Observation of an All-Boron Fullerene. *Nature Chem.* **2014**, *6*, 727-731.

(4) Chen, Q.; Li, W.L.; Zhao, Y. F.; Zhang, S. Y.; Hu, H. S.; Bai, H.; Li, H. R.; Tian, W. J.; Lu, H. G.; Zhai, H. J., Experimental and Theoretical Evidence of an Axially Chiral Borospherene. *ACS Nano* **2014**, *9*, 754-760.

(5) Wang, Y. J.; Zhao, Y. F.; Li, W. L.; Jian, T.; Chen, Q.; You, X. R.; Ou, T.; Zhao, X. Y.; Zhai, H. J.; Li, S. D., Observation and Characterization of the Smallest Borospherene, B_{28}^- and B_{28}. *J. Chem. Phys.* **2016**, *144*, 064307.

(6) Zhao, J.; Wang, L.; Li, F.; Chen, Z., B_{80} and Other Medium-Sized Boron Clusters: Core− Shell Structures, Not Hollow Cages. *J. Phys. Chem. A* **2010**, *114*, 9969-9972.

(7) Rahane, A. B.; Kumar, V., B 84: A Quasi-Planar Boron Cluster Stabilized with Hexagonal Holes. *Nanoscale* **2015**, *7*, 4055-4062.

(8) Kiran, B.; Bulusu, S.; Zhai, H. J.; Yoo, S.; Zeng, X. C.; Wang, L. S., Planar-to-Tubular Structural Transition in Boron Clusters: B_{20} as the Embryo of Single-Walled Boron Nanotubes. *Proc. Nat. Acad. Sci. of the United States of America* **2005**, *102*, 961-964.

(9) Chacko, S.; Kanhere, D. G.; Boustani, I., Ab Initio Density Functional Investigation of B_{24} Clusters: Rings, Tubes, Planes, and Cages. *Phys. Rev. B* **2003**, *68*, 035414.

(10) Singh, A. K.; Briere, T. M.; Kumar, V.; Kawazoe, Y., Magnetism in Transition-Metal-Doped Silicon Nanotubes. *Phys. Rev. Lett.* **2003**, *91*, 146802.

(11) Singh, A. K.; Kumar, V.; Briere, T. M.; Kawazoe, Y., Cluster Assembled Metal Encapsulated Thin Nanotubes of Silicon. *Nano Lett.* **2002**, *2*, 1243-1248.

(12) Jian, T.; Li, W. L.; Popov, I. A.; Lopez, G. V.; Chen, X.; Boldyrev, A. I.; Li, J.; Wang, L. S., Manganese-Centered Tubular Boron Cluster– MnB_{16}^-: A New Class of Transition-Metal Molecules. *J. Chem. Phys.* **2016**, *144*, 154310.

(13) Popov, I. A.; Jian, T.; Lopez, G. V.; Boldyrev, A. I.; Wang, L. S., Cobalt-Centred Boron Molecular Drums with the Highest Coordination Number in the CoB_{16}^- Cluster. *Nature Commun.* **2015**, *6*.

(14) Sergeeva, A. P.; Zubarev, D. Y.; Zhai, H. J.; Boldyrev, A. I.; Wang, L. S., A Photoelectron Spectroscopic and Theoretical Study of B_{16}^- and B_{16}^{2-}: An All-Boron Naphthalene. *J. Am. Chem. Soc.* **2008**, *130*, 7244-7246.

(15) Kumar, V.; Singh, A. K.; Kawazoe, Y., Smallest Magic Caged Clusters of Si, Ge, Sn, and Pb by Encapsulation of Transition Metal Atom. *Nano Lett.* **2004**, *4*, 677-681.

(16) Xu, C.; Cheng, L.; Yang, J., Double Aromaticity in Transition Metal Centered Double-Ring Boron Clusters M@B_{2n} (M= Ti, Cr, Fe, Ni, Zn; n= 6, 7, 8). *J. Chem. Phys.* **2014**, *141*, 124301.

(17) Lv, J.; Wang, Y.; Zhang, L.; Lin, H.; Zhao, J.; Ma, Y., Stabilization of Fullerene-Like Boron Cages by Transition Metal Encapsulation. *Nanoscale* **2015**, *7*, 10482-10489.

(18) Saha, P.; Rahane, A. B.; Kumar, V.; Sukumar, N., Analysis of the Electron Density Features of Small Boron Clusters and the Effects of Doping with C, P, Al, Si, and Zn: Magic B_7P and B_8Si Clusters. *Phys. Scripta* **2016**, *91*, 053005.

(19) Czekner, J.; Cheung, L.-F.; Wang L.-S., Probing the Structures of Neutral B11 and B12 Using High Resolution Photoelectron Imaging of $B11^-$ and $B12^-$, *J. Phys. Chem. C*, just accepted, DOI: 10.1021/acs.jpcc.6b10958.

(20) Cheng, L., B14: An All-Boron Fullerene. *J. Chem. Phys.* **2012**, *136*, 104301.

(21) Ekardt, W., Work Function of Small Metal Particles: Self-Consistent Spherical Jellium-Background Model. *Phys. Rev. B* **1984**, *29*, 1558.

(22) Koskinen, M.; Lipas, P. O.; Manninen, M., Electron-Gas Clusters: The Ultimate Jellium Model. *Z. Phys. D Atoms, Molecules and Clusters* **1995**, *35*, 285-297.

23) Singh, A.K.; Kumar, V.; Kawazoe, Y., Metal encapsulated nanotubes of silicon and germanium, *J. Mater. Chem.* **2004**, *14*, 555-563.

24) Singh, A.K.; Kumar, V.; Kawazoe, Y., Metal encapsulated nanotubes of germanium with metal dependent electronic properties, *Eur. Phys. J. D - Atomic, Molecular, Optical and Plasma Physics* **2005**, *34*, 295-298.

(25) Perdew, J. P.; Burke, K.; Ernzerhof, M., *Phys. Rev. Lett.* 77: 3865. *Errata:(1997) Phys. Rev. Lett.* **1996**, *78*, 1396.

(26) Kresse, G.; Furthmüller, J., Efficiency of Ab-Initio Total Energy Calculations for Metals and Semiconductors Using a Plane-Wave Basis Set. *Comp. Mater. Sci.* **1996**, *6*, 15-50.

(27) Kresse, G.; Furthmüller, J., Efficient Iterative Schemes for Ab Initio Total-Energy Calculations Using a Plane-Wave Basis Set. *Phys. Rev. B* **1996**, *54*, 11169.

(28) Frisch, M. J.; Trucks, G. W.; Schlegel, H. B.; Scuseria, G. E.; Robb, M. A.; Cheeseman, J. R.; Scalmani, G.; Barone, V.; Mennucci, B.; Petersson, G. A., Gaussian 09, Rev. A. 1. Wallingford, Ct: Gaussian. Inc: 2009.

(29) Gatti, C.; Cargnoni, F.; Bertini, L., Chemical Information from the Source Function, *J. Comp. Chem.* **2003**, *24*, 422-436.

(30) Gatti, C.; Orlando, A.M.; Monza, E.; Presti, L.L., Exploring Chemistry Through the Source Function for the Electron and the Electron Spin Densities, in Chauvin R. *et al.* (eds.), Applications of Topological Methods in Molecular Chemistry, Challenges and Advances in Computational Chemistry and Physics **2016**, 22, Springer International Publishing Switzerland.

(31) Gatti, C.; Saleh, G.; Presti, L.L., Source Function applied to experimental densities reveals subtle electron-delocalization effects and appraises their transferability properties in crystals, *Acta Cryst.* **2016**, B72, 180–193.

(32) Gatti, C.; Bertini, L., The local form of the source function as a fingerprint of strong and weak intra- and intermolecular interactions, *Acta Cryst.* **2004**, A60, 438-449.

(33) Keith, T. A., Aimall (Version 11.03. 14), 2011. *Available via DIALOG at: http://aim. tkgristmill.com Search PubMed* **2012**.

(34) Sumar, I.; Cook, R.; Ayers, P. W.; Matta, C. F., AIMldm: A Program to Generate and Analyze Electron Localization–Delocalization Matrices (Ldms). *Comp. Theor. Chem.* **2015**, *1070*, 55-67.

(35) Timm, M.J.; Matta, C.F.; Massa, L.; Huang, L., The Localization−Delocalization Matrix and the Electron-Density-Weighted Connectivity Matrix of a Finite Graphene Nanoribbon Reconstructed from Kernel Fragments, *J. Phys. Chem. A* **2014**, 118, 11304−11316.

(36) Becke, A. D.; Edgecombe, K. E., A Simple Measure of Electron Localization in Atomic and Molecular Systems. *The J. Chem. Phys.* **1990**, *92*, 5397-5403

Table of Contents Graphic

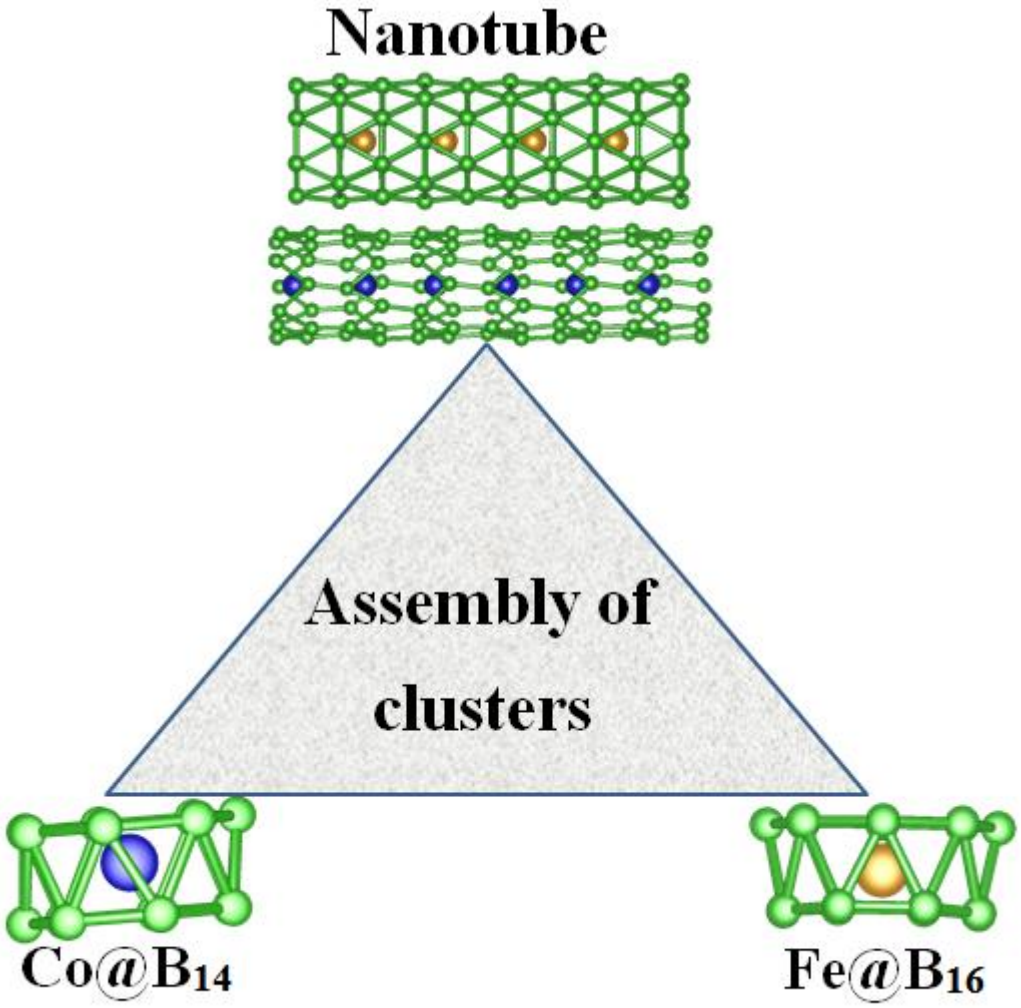

Drum-shaped $Co@B_{14}$ and $Fe@B_{16}$ stable clusters that can be assembled to form carbon-like nanotube with boron hexagons and a nanotube with triangular boron network, respectively.